J. Fluid Mech. (1999), *vol.* 401, *pp.* 243–274. Printed in the United Kingdom

© 1999 Cambridge University Press

Self-diffusion in sheared suspensions by dynamic simulation

By DAVID R. FOSS AND JOHN F. BRADY

Division of Chemistry and Chemical Engineering, California Institute of Technology, Pasadena, CA 91125, USA

(Received 2 February 1999 and in revised form 26 July 1999)

The behaviour of the long-time self-diffusion tensor in concentrated colloidal dispersions is studied using dynamic simulation. The simulations are of a suspension of monodisperse Brownian hard spheres in simple shear flow as a function of the Péclet number, *Pe*, which measures the relative importance of shear and Brownian forces, and the volume fraction, ϕ. Here, $Pe = \dot{\gamma}a^2/D_0$, where $\dot{\gamma}$ is the shear rate, a the particle size and $D_0 = kT/6\pi\eta a$ is the Stokes–Einstein diffusivity of an isolated particle of size a with thermal energy kT in a solvent of viscosity η. Two simulations algorithms are used: Stokesian Dynamics for inclusion of the many-body hydrodynamic interactions, and Brownian Dynamics for suspensions without hydrodynamic interactions. A new procedure for obtaining high-quality diffusion data based on averaging the results of many short simulations is presented and utilized. At low shear rates, low *Pe*, Brownian diffusion due to a random walk process dominates and the characteristic scale for diffusion is the Stokes–Einstein diffusivity, D_0. At zero *Pe* the diffusivity is found to be a decreasing function of ϕ. As *Pe* is slowly increased, $O(Pe)$ and $O(Pe^{3/2})$ corrections to the diffusivity due to the flow are clearly seen in the Brownian Dynamics system in agreement with the theoretical results of Morris & Brady (1996). At large shear rates, large *Pe*, both systems exhibit diffusivities that grow linearly with the shear rate by the non-Brownian mechanism of shear-induced diffusion. In contrast to the behaviour at low *Pe*, this shear-induced diffusion mode is an increasing function of ϕ. Long-time rotational self-diffusivities are of interest in the Stokesian Dynamics system and show similar behaviour to their translational analogues. An off-diagonal long-time self-diffusivity, D_{xy}, is reported for both systems. Results for both the translational and rotational D_{xy} show a sign change from low *Pe* to high *Pe* due to different mechanisms in the two regimes. A physical explanation for the off-diagonal diffusivities is proposed.

1. Introduction

This work addresses the problem of determining the long-time self-diffusivity in a monodisperse low-Reynolds-number suspension of spherical particles at equilibrium and under steady shear conditions via dynamic simulation. Self-diffusion is one of the most basic transport processes occurring in a suspension and is related to a number of transport and relaxation mechanisms. There are three well-defined diffusive processes in a colloidal suspension: the short-time self-diffusivity, D_0^s, the long-time self-diffusivity, D_∞^s, and the gradient or collective diffusivity, D^c. At infinite dilution all three diffusivities are the same and equal to the Stokes–Einstein diffusivity of an isolated particle: $D_0 = kT/6\pi\eta a$ for translational self-diffusion and $D_0^r =$

https://doi.org/10.1017/S0022112099006576 Published online by Cambridge University Press

$kT/8\pi\eta a^3$ for its rotational analogue. Here, k is Boltzmann's constant, T is the absolute temperature, η is the viscosity of the continuum suspending fluid, and a is the characteristic particle size, which for a monodisperse suspension of spheres is simply the particle radius.

As the concentration is increased and the effects of particle interactions become important, the three diffusivities behave quite differently as they represent three distinct physical processes. The short-time self-diffusivity measures the local particle mobility on time scales long compared to the momentum relaxation time, $\tau_I = m/6\pi\eta a$, but small compared to the time it takes for a particle to move a fraction of its size, which is the diffusive time scale, $\tau_D = a^2/D_0$; here, m is the mass of the particle. The long-time self-diffusivity is related to diffusion on times long compared to a^2/D_0, so that a particle has wandered far from its starting point. Finally, the gradient or collective diffusivity results from a flux down a macroscopic concentration gradient. This work focuses on the long-time self-diffusivity.

While the short-time self-diffusivity depends only on the particle mobility, which is a purely time-independent hydrodynamic quantity, the long-time self-diffusivity is affected by both the particle mobility and the dynamic microstructure of particles exchanging places with their neighbours. Often researchers have simplified the system by excluding hydrodynamic interactions, which sets the mobility of each particle to unity and independent of microstructural variations, effectively isolating the contribution of the dynamic microstructure to the long-time self-diffusivity. A Brownian Dynamics algorithm is employed for the simplified system of hard spheres interacting in the absence of hydrodynamic interactions. For the complete system, the computationally intensive Stokesian Dynamics algorithm that includes the many-body hydrodynamic interactions into the Brownian Dynamics framework is used. A goal of this work is to compare and contrast results from these two systems to provide insight into the relevant mechanisms for long-time self-diffusion.

Much work has been done on the long-time self-diffusivity at both equilibrium and in the high-shear limit. Dynamic light scattering can be used to measure the self-diffusivity at equilibrium, while tracer experiments, where a small fraction of the particles are tagged and their motion monitored, can be used, in principle, at any shear rate, although only experiments at high shear rates have been performed to date. Out of equilibrium, structural anisotropies arise due to the shearing flow and the long-time self-diffusivity is properly represented in full tensorial form, $\boldsymbol{D}^s_\infty$, whose components are defined using a Cartesian coordinate system, (x, y, z), with principal axes corresponding to the velocity, velocity-gradient, and vorticity directions in simple shear flow, respectively.

Theoretical work on self-diffusion at high shear rates is complicated by the fact that two particles acting solely under the influence of hydrodynamics exhibit no diffusive behaviour due to the symmetry properties of low-Reynolds-number flow. Wang, Mauri & Acrivos (1996) examined self-diffusion in dilute suspensions theoretically using three-particle interactions. da Cunha & Hinch (1996) examined the two-particle problem, adding surface roughness to create diffusive motion. Brady & Morris (1997) used residual Brownian motion and hard-sphere interparticle forces to break the symmetry of the pure hydrodynamic limit. Effects of weak shear on self-diffusion were studied by Morris & Brady (1996). The last two studies are referred to many times throughout this paper and will be discussed in more detail in § 2. One interesting prediction of these works is the appearance of a non-zero off-diagonal or xy-component of the long-time self-diffusivity tensor in simple shear flow. This quantity is difficult to measure both experimentally and via simulation as it involves

https://doi.org/10.1017/S0022112099006576 Published online by Cambridge University Press

examining motion in the direction of the bulk flow. The current work makes use of a method for calculating the diffusivity that enables us to obtain meaningful results for this quantity.

We also present results for the long-time rotational diffusivity. Theoretical work by Jones (1989) and Degiorgio, Piazza & Jones (1995) predict behaviour for dilute suspensions at equilibrium considering two- and three-body hydrodynamic interactions. Short-time rotational diffusivities at equilibrium for all volume fractions were determined by Stokesian Dynamics simulations by Phillips, Brady & Bossis (1988). Many advances have been made recently in experimentally measuring rotational self-diffusion using techniques ranging from dynamic depolarized light scattering (Degiorgio *et al.* 1995), forced Rayleigh scattering (Kanetakis & Sillescu 1996), and nuclear magnetic resonance spectroscopy (Barrall *et al.* 1996; Kanetakis, Tölle & Sillescu 1997). To date, work has been performed at equilibrium with extensive focus on the behaviour of the short-time rotational self-diffusivity over a wide range of volume fraction, ϕ.

In the next section we discuss the theoretical results of Morris & Brady (1996) and Brady & Morris (1997), analysing what behaviour is to be expected in shear flow. Section 3 outlines the simulation method, discussing the two simulation techniques used, how the diffusion coefficients are calculated, and a new way of splitting the diffusivity into its hydrodynamic and Brownian contributions. In § 4, results for the diagonal components of the long-time self-diffusion tensor are presented showing their dependence on both density and shear rate. The simulation results are shown to compare well with experimental data. Section 5 is devoted to discussing the off-diagonal components of the self-diffusion tensor and presenting possible physical mechanisms for this mode of diffusion. Finally, we conclude in § 6 with a summary and suggestions for future studies.

2. Theoretical background

According to the theoretical results of Morris & Brady (1996), at small shear rates in the absence of hydrodynamic interactions, the long-time self-diffusion tensor of colloidal suspensions has the following form:

$$\boldsymbol{D}^s_\infty = D_0[(1-2\phi)\boldsymbol{I} + \tfrac{46}{15}\phi(\tfrac{1}{2}Pe)\hat{\boldsymbol{E}} + 0.65\phi(\tfrac{1}{2}Pe)^{3/2}\boldsymbol{I} + O(\phi^2, Pe^2)], \tag{1}$$

where the Péclet number $Pe = \dot\gamma a^2/D_0 = 6\pi\eta a^3\dot\gamma/kT$ and $\dot\gamma$ is the shear rate. The non-dimensional rate of strain tensor is $\hat{\boldsymbol{E}} = \boldsymbol{E}/\dot\gamma$, and $\boldsymbol{I}$ is the isotropic tensor. This result is strictly valid to leading order in volume fraction, ϕ, but the general form may be applicable at higher concentrations. The $O(Pe)$ contribution is valid for a general linear flow and represents a correction to the diffusion due to a perturbed microstructure. For weak flows, there is an $O(Pe)$ deformation to the equilibrium microstructure that scales as $Pe\hat{\boldsymbol{E}}$. This perturbation causes a volume fraction fluctuation of $-\phi Pe\hat{\boldsymbol{E}}$ around a particle; there is a buildup of particles in the compressional zones and a depletion of particles in the extensional zones (Batchelor 1977). For a simple random walk in the perturbed microstructure, we obtain the $\phi Pe\hat{\boldsymbol{E}}$ correction to the diffusivity. The $O(Pe^{3/2})$ term for simple shear flow is isotropic, and represents the first contribution to the normal components of the long-time self-diffusion tensor. This term results from a singular effect of weak advection at large separations, $r/a \sim O(Pe^{-1/2})$ (Leal 1973), and can be clearly seen in figure 4.

Morris & Brady (1996) also studied the effect of including hydrodynamic interactions on diffusion. For small Pe, the long-time self-diffusion tensor in a dilute

https://doi.org/10.1017/S0022112099006576 Published online by Cambridge University Press

suspension behaves as

$$\boldsymbol{D}^s_\infty = D_0[(1-2.07\phi)\boldsymbol{I} + 0.30\phi(\tfrac{1}{2}Pe)\hat{\boldsymbol{E}} + \mathscr{D}\phi(\tfrac{1}{2}Pe)^{3/2} + O(\phi^2, Pe^2)], \tag{2}$$

where, for simple shear flow,

$$\mathscr{D} = \begin{pmatrix} 3.96 & 0.93 & 0 \\ 0.93 & 1.87 & 0 \\ 0 & 0 & 0.52 \end{pmatrix}.$$

Equation (2) has the same general form as (1) with a few exceptions. The equilibrium isotropic term and the $O(Pe)$ term valid for general linear flow have different coefficients and show a hindrance of the diffusion process on the inclusion of hydrodynamic interactions. Also, the $O(Pe^{3/2})$ contribution is no longer isotropic, not only showing different contributions along the diagonal but also a significant positive contribution to the off-diagonal xy-component.

The behaviour at high Pe has also been analysed theoretically by Brady & Morris (1997) and da Cunha & Hinch (1996). Brady & Morris (1997) find that the long-time diffusivity for monodisperse hard spheres in the absence of hydrodynamic interactions is related to the particle contribution to the stress, Σ, by the following relation:

$$\boldsymbol{D}^s_\infty = -\frac{a^2}{\eta}\frac{1}{\phi}\frac{2}{27}\Sigma, \tag{3}$$

which supports the idea of self-diffusion being driven by the osmotic, or partial, pressure: the self-diffusivity is the product of the particle mobility, which is $O(1)$ in the absence of hydrodynamic interactions, and the osmotic pressure gradient $\partial\Sigma/\partial\phi$. The coefficient $\frac{2}{27}$ in (3) is strictly valid only for dilute suspensions, but the origin of the asymmetry that gives rise to the diffusion process is in a singular boundary layer at particle contact and thus the proportionality in (3) should be valid for all ϕ. From this relation we can come to several conclusions about the long-time diffusivity. First, since all components of the stress tensor scale as $\eta\dot{\gamma}$ in the high shear limit, all diffusivities scale as $\dot{\gamma}a^2$, as simple dimensional reasoning would suggest. Second, the simple radial-balance approximation used by Brady & Morris (1997) predicts a zero first normal stress difference, $N_1 = \Sigma_{xx} - \Sigma_{yy}$, as well as a negative second normal stress difference, $N_2 = \Sigma_{yy} - \Sigma_{zz}$. The normal stress differences lead to the inequality $\Sigma_{zz} > \Sigma_{yy} \approx \Sigma_{xx}$, which due to the minus sign in (3), gives long-time self-diffusivities of the following relative magnitudes: $D_{xx} \approx D_{yy} > D_{zz}$. Also, there is a positive off-diagonal component to the stress tensor Σ_{xy} – the shear stress is non-zero – resulting in a negative value of D_{xy}. These simple high-Péclet-number predictions are born out in the Brownian Dynamics simulation. (cf. figures 3 and 19).

The inclusion of hydrodynamic interactions complicates matters in an important way. The pure-hydrodynamic limit corresponding to hydrodynamic interactions only, no Brownian motion nor interparticle forces, is a singular limit and, for two particles, exhibits no diffusion due to the symmetry and reversibility of low-Reynolds-number flow. The symmetry can easily be broken, however, by the presence of other forces, whether they are due to Brownian motion or to a repulsive interparticle force of non-hydrodynamic origin, no matter how small in magnitude. The simple relationship between diffusivity and stress in (3) no longer holds due to the complexity of the hydrodynamic interactions. However, the diffusivity can still be thought of as a particle mobility times an osmotic pressure gradient, but the particle mobility is no longer a constant due to the presence of lubrication forces near contact. Apart from the special case of the pure hydrodynamic limit, the principal effect of hydrodynamic interactions

https://doi.org/10.1017/S0022112099006576 Published online by Cambridge University Press

is the quantitative dependence of the diffusivity on the volume fraction ϕ. The first normal stress difference, N_1, is no longer zero and has been shown by simulation to be negative. This leads the inequality $\Sigma_{zz} > \Sigma_{yy} > \Sigma_{xx}$, which results in diffusivities of the following magnitudes: $D_{xx} > D_{yy} > D_{zz}$. As before, the sole off-diagonal contribution is a negative D_{xy}. Figures 5 and 21 show that these simple predictions at high Péclet number are born out in the Stokesian Dynamics simulations.

3. Simulation method

Long-time self-diffusivities were determined with and without hydrodynamics using Stokesian Dynamics and Brownian Dynamics simulations, respectively. Brownian Dynamics is appropriate for particles interacting through long-range repulsive forces such that the thermodynamic volume fraction – based on the radius of the overlapping repulsive forces – is much larger than the hydrodynamic volume fraction – based on the actual size of the particles. Stokesian Dynamics, since it includes hydrodynamics, is applicable in general no matter what the form or range of interparticle forces; indeed, Brownian Dynamics is a special limiting case of Stokesian Dynamics. Rather than focusing on specific systems, however, the point of conducting both Brownian and Stokesian Dynamics simulations is to try to separate the geometric and statistical effects, which are present in both methods, from the hydrodynamic effects, which are only present in Stokesian Dynamics. We shall see that provided the suspension is disordered (a state that cannot be reached at high Péclet number with Brownian Dynamics as discussed below) hydrodynamics apparently has only a quantitative effect (cf. figures 11 and 14).

We shall not focus on the details of these two techniques, as they are found elsewhere, but rather give a brief overview of each, and then discuss how they were implemented to compute the long-time self-diffusivities. The Brownian Dynamics algorithm used here is based on the method of Heyes & Melrose (1993) and Schaertl & Sillescu (1994). Measurement of the long-time self-diffusivities involves calculation of the mean-square displacements of each particle over time, which are calculated from the individual particle trajectories. These trajectories are governed by the particle evolution equation for this system:

$$\Delta \boldsymbol{x} = \Delta \boldsymbol{x}^{a} + \Delta \boldsymbol{x}^{HS} + \boldsymbol{X}(\Delta t), \tag{4a}$$

$$\overline{\boldsymbol{X}} = 0 \quad \text{and} \quad \overline{\boldsymbol{X}(\Delta t)\boldsymbol{X}(\Delta t)} = 2D_0 \boldsymbol{I} \Delta t. \tag{4b}$$

Here, $\Delta \boldsymbol{x}^{a} = \boldsymbol{U}\Delta t$ is the affine contribution due to the bulk shear flow and is simply $\dot{\gamma} y \hat{\boldsymbol{i}} \Delta t$ for simple shear flow. The random Brownian step, $\boldsymbol{X}$, has zero mean (denoted by the overbar) and variance equal to the single-particle Stokes–Einstein diffusivity, D_0, in the absence of hydrodynamic interactions. After the affine and Brownian contributions are added, the algorithm searches for particle pairs that have overlapped during the time step Δt and displaces each particle $\Delta \boldsymbol{x}^{HS}$ along their line of centres returning the particles to contact in response to a hard-sphere-like interparticle force. There is a small inherent 'softness' to the interparticle potential due to three-body effects that are not resolved using this method, but these systems have been shown to mimic the behaviour of hard spheres in several regards. The shear stress autocorrelation function is found to diverge at short times as $t^{-1/2}$, the osmotic pressure as a function of ϕ shows good agreement with the hard-sphere equation of state, and the equilibrium radial-distribution function agrees with the known form for hard spheres (Foss 1999). The simplicity of the algorithm used in this

https://doi.org/10.1017/S0022112099006576 Published online by Cambridge University Press

work allows for systems with large numbers of particles ($N = 1331$, in this study), reducing the statistical noise. Hard-sphere suspensions can also be approximated using a steep, continuous, interparticle potential, such as r^{-n}, where n is made very large. These algorithms produce very large values of the interparticle force near contact which necessitates the use of an extremely small time step in order to prevent an unrealistically large particle displacement during a typical particle collision.

In simple-shear flow, the mean-square displacements are expected to grow with time according to those for diffusion from a point source (Elrick 1962; Morris & Brady 1996):

$$\langle x^2(t)\rangle = 2D_{xx}t + 2D_{yy}t\ [1 + \tfrac{1}{3}(\dot{\gamma}t)^2], \tag{5a}$$

$$\langle y^2(t)\rangle = 2D_{yy}t, \tag{5b}$$

$$\langle z^2(t)\rangle = 2D_{zz}t, \tag{5c}$$

$$\langle x(t)y(t)\rangle = 2D_{xy}t + D_{yy}t(\dot{\gamma}t), \tag{5d}$$

as $t \to \infty$. Here the angle brackets $\langle\ \rangle$ denote an average over all particles in the system. The diffusivity in the velocity-gradient direction, D_{yy}, provides not only the normal diffusive behaviour in the y-direction, but also couples with the motion in the x-direction, resulting in $\langle x^2(t)\rangle$ growing cubically with time and $\langle x(t)y(t)\rangle$ growing quadratically in time, both with a proportionality constant given by D_{yy}. The underlying linear growth represented by the presence of D_{xx} and D_{xy} is dominated by the convectively enhanced stronger growths of the $\langle x^2(t)\rangle$ and $\langle x(t)y(t)\rangle$ displacements, making these diffusivities computationally difficult to measure. To circumvent this problem, we can take advantage of the fact that in simulation we know precisely the affine displacement at each time step, $\Delta\boldsymbol{x}^a$ in (4a). By subtracting off the affine displacement at each instant as far as the mean-square displacement is concerned, we can remove this nonlinear temporal growth and extract all components, D_{yy}, D_{xx}, D_{zz} and D_{xy}. Note, as far as the suspension structure and dynamics are concerned, the affine displacement is, of course, added; it is only removed to compute $\boldsymbol{D}^s_\infty$. Thus, the long-time self-diffusivity is given by

$$\boldsymbol{D}^s_\infty = \lim_{t\to\infty} \frac{1}{2}\frac{\mathrm{d}}{\mathrm{d}t}\langle(\boldsymbol{x}(t) - \boldsymbol{x}^a(t))(\boldsymbol{x}(t) - \boldsymbol{x}^a(t))\rangle, \tag{6}$$

where $\boldsymbol{x}^a(t)$ represents the affine contribution to a particle's displacement. This approach of subtracting off the affine displacement was also used successfully by Sami (1996) in extensional flow, where the temporal growth of the convectively enhanced dispersion is now exponential rather than a power law.

The inclusion of hydrodynamics, which includes both the many-body far-field interactions and the pairwise-additive lubrication forces between particles, necessitates the use of the Stokesian Dynamics simulation technique described in detail elsewhere (Bossis & Brady 1987; Brady & Bossis 1988). The computational cost of calculating all the hydrodynamic interactions in conventional Stokesian Dynamics is $O(N^3)$, and thus we are limited to relatively small system sizes (generally $N = 27$). As before, the particle-evolution equation contains all the vital information for calculating the mean-square displacements. Previously, the particle stress was shown to consist of both hydrodynamic and Brownian contributions (Bossis & Brady 1989), and the particle trajectories are no different. For Stokesian Dynamics, it is useful to write the

https://doi.org/10.1017/S0022112099006576 Published online by Cambridge University Press

evolution equation as

$$\Delta \boldsymbol{x} = \Delta \boldsymbol{x}^{a} + \Delta \boldsymbol{x}^{H} + \Delta \boldsymbol{x}^{B}. \tag{7}$$

Here, we have broken the evolution equation into three contributions. The first is the affine displacement:

$$\Delta \boldsymbol{x}^{a} = \boldsymbol{U}\Delta t = \dot{\gamma} y \hat{\boldsymbol{i}} \Delta t, \tag{8}$$

which simply advects the particle along with the bulk shear flow. The second contribution, the hydrodynamic displacement, is given as

$$\Delta \boldsymbol{x}^{H} = \boldsymbol{R}_{FU}^{-1} \boldsymbol{\cdot} \boldsymbol{R}_{FE} \,\boldsymbol{:} \boldsymbol{E}\, \Delta t. \tag{9}$$

Here, $\boldsymbol{R}_{FU}$ and $\boldsymbol{R}_{FE}$ are configuration-dependent hydrodynamic resistance tensors. These displacements describe the deviation in particle paths from the affine motion solely due to hydrodynamic interactions. The remaining contribution to the particle evolution equation is the Brownian displacement, originally given by Ermak & McCammon (1978) as

$$\Delta \boldsymbol{x}^{B} = kT \nabla \boldsymbol{\cdot} \boldsymbol{R}_{FU}^{-1} \Delta t + \boldsymbol{X}(\Delta t), \tag{10a}$$

$$\overline{\boldsymbol{X}} = 0 \quad \text{and} \quad \overline{\boldsymbol{X}(\Delta t)\boldsymbol{X}(\Delta t)} = 2kT \boldsymbol{R}_{FU}^{-1} \Delta t. \tag{10b}$$

Here, the short-time self-diffusion tensor enters as $kT\boldsymbol{R}_{FU}^{-1}$ (which is just the Stokes–Einstein diffusivity using the many-body hydrodynamic mobility, $\boldsymbol{R}_{FU}^{-1}$, instead of the single-particle inverse Stokes drag) as the variance of the random step $\boldsymbol{X}$. Also, because the random step is large, $O(\Delta t^{1/2})$, compared to the $O(\Delta t)$ size of the hydrodynamic and affine displacements, a higher-order term including the spatial gradient of the short-time diffusion tensor must be included to account for changes in the particle mobility during the random step. This deterministic term acts as a radially repulsive force and helps to prevent particles from overlapping during a random step. No interparticle forces of non-hydrodynamic origin are required in order to prevent particle overlaps and no such forces are included in Stokesian Dynamics simulations.

All positions $\boldsymbol{x}$ are non-dimensionalized by the particle radius a, the rate-of-strain tensor $\boldsymbol{E}$ by its magnitude $\dot{\gamma}$, the imposed velocity $\boldsymbol{U}$ by $\dot{\gamma}a$ and the hydrodynamic resistance tensors $\boldsymbol{R}_{FU}$ and $\boldsymbol{R}_{FE}$ by $6\pi\eta a$ and $6\pi\eta a^2$, respectively. There are two characteristic time scales: the time scale for the affine and hydrodynamic displacements is the flow time scale, $\dot{\gamma}^{-1}$, whereas the relevant time scale for the Brownian displacements is the diffusive time scale, $a^2/D_0 = 6\pi\eta a^3/kT$. The ratio of the diffusive time scale to the flow time scale is the Péclet number, $Pe = \dot{\gamma}a^2/D_0$. Thus, one can think of the random Brownian displacements as those that are present at equilibrium in the absence of flow ($Pe = 0$), and the hydrodynamic displacements as those that accompany the affine flow in the pure hydrodynamic limit ($Pe^{-1} \equiv 0$). This non-dimensionalization applies to both the Stokesian Dynamics and Brownian Dynamics systems and the Péclet number is also the appropriate non-dimensional shear rate for the Brownian Dynamics system (4*a*).

The pure hydrodynamic limit – no Brownian motion and no interparticle forces – is singular and in order to resolve the strong lubrication forces between the particles an infinitesimally small time step is required resulting in prohibitive computational cost (Ball & Melrose 1995; Dratler & Schowalter 1996). Inclusion of a non-hydrodynamic interparticle repulsive force is often used to study non-Brownian suspensions (Yurkovetsky 1998); here, we shall limit ourselves to large, but finite, Pe, where residual Brownian motion is sufficient to prevent particle overlaps with a serviceably finite simulation time step. The fact that there are no interparticle forces may have implications for the resulting diffusivity, however.

https://doi.org/10.1017/S0022112099006576 Published online by Cambridge University Press

As with Brownian Dynamics, the particle mean-square displacements are calculated as a function of time ignoring the affine displacements to eliminate nonlinear temporal behaviour. Here, we have the advantage of separating the hydrodynamic and random Brownian contributions,

$$\langle (\boldsymbol{x} - \boldsymbol{x}^a)(\boldsymbol{x} - \boldsymbol{x}^a) \rangle = \langle \boldsymbol{x}^H \boldsymbol{x}^H \rangle + \langle \boldsymbol{x}^B \boldsymbol{x}^B \rangle + [\langle \boldsymbol{x}^H \boldsymbol{x}^B \rangle + \langle \boldsymbol{x}^B \boldsymbol{x}^H \rangle]. \tag{11}$$

Unlike the particle displacements, the square displacements are not additive and a symmetric cross-correlation term between hydrodynamic and random Brownian displacements appears. Comparing (11) to (6) we can define

$$\boldsymbol{D}^s_\infty = \boldsymbol{D}^s_{\infty,h} + \boldsymbol{D}^s_{\infty,b} + \boldsymbol{D}^s_{\infty,hb}, \tag{12}$$

providing useful knowledge of the individual contributions to the long-time self-diffusion tensor. This division of diffusivities is not possible in Brownian Dynamics due to the inclusion of the hard-sphere-like interparticle force which acts in the same manner in response to both Brownian and affine motion and thus cannot itself be separated into Brownian and non-Brownian components.

One might question the validity of dividing the displacements in such a manner. In separating the hydrodynamic and Brownian displacements we do not claim that each one is acting independently of the other. Clearly, the two are acting together to create a dynamic microstructure that in turn affects the temporal behaviour of the trajectories of each particle. Separation of the displacements is a relatively simple matter in the context of a computer simulation, however, and provides some insight into the mechanisms for self-diffusion.

Calculation of the mean-square displacement curves for both Brownian Dynamics and Stokesian Dynamics is done with the aid of a novel method. First, the simulations are kept relatively short, that is, for a time sufficient for the system to reach a steady state and for the mean-square displacements to enter the linear regime for an appreciable length of time. Second, many of these short simulations are performed independently from separate initial hard-sphere equilibrium configurations, creating a large number of mean-square displacement curves. All of these curves are then averaged together point by point to form one smooth mean-square displacement curve. Figure 1 shows that times up to a strain of 1 or 2 are sufficient to achieve a linear growth in the mean-square displacement. In a like manner, stresses have reached their steady state in a strain of 1.

This method works well for four reasons. First, averaging over many runs reduces the costly $N^{-1/2}$ noise present in random walk calculations. This is especially advantageous when using Stokesian Dynamics as the cost of increasing the system size is high. Second, although averaging over long times is useful in obtaining good data in finite systems for properties with well-defined instantaneous values such as stresses and spatial distribution functions, it often creates problems in time-dependent correlations such as Green–Kubo auto-correlation functions and mean-square displacements. These quantities continue to directly depend on – instead of becoming independent of – the initial condition of the system. For this reason the statistical noise in these functions grows with time. More realizations, i.e. averaging over many correlations from different starting points, is used to obtain better quality autocorrelation functions, but the long-time 'tails' of these functions are very difficult to measure accurately. This is true for mean-square displacements for the same physical reasons. As a particle has diffused far from its starting point the instantaneous random fluctuations of the particle have very little dependence on the initial particle position and thus show large fluctuations in the mean-square displacement curve. The use of many realizations can

https://doi.org/10.1017/S0022112099006576 Published online by Cambridge University Press

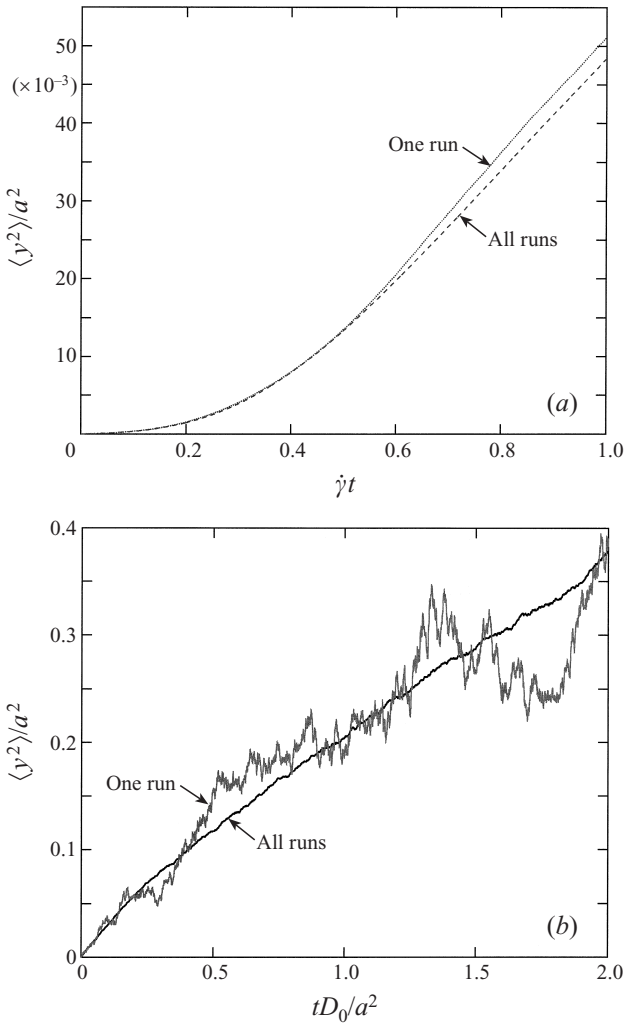

FIGURE 1. Mean-square displacements as a functions of time (*a*) for the Brownian Dynamics system for $\phi = 0.45$, $Pe = 1000$ and (*b*) Stokesian Dynamics system for $\phi = 0.45$, $Pe = 0.3$, comparing data using both one and all realizations.

delay the onset of this noise, whether it be by frequently resetting the starting point, or by increasing the number of particles, but the noise will always persist at long times.

This brings us to the third point: analysis of the mean-square displacement curves at very long times is not necessary because it does not require a very long time for the mean-square displacements to reach their linear, long-time asymptote. This may seem counterintuitive due to the infinite time limit present in (6), but a particle does not have to travel long distances in order to reach its long-time asymptote; it simply has to encounter enough particle–particle interactions to sample the dynamic microstructure present. In the familiar cage-diffusion model, the particle does not have to leave the cage and travel far from its starting point, it simply has to interact with enough of its neighbouring cage members until all the information necessary for long-time diffusion has been attained. This idea has been born out by the recent

https://doi.org/10.1017/S0022112099006576 Published online by Cambridge University Press

experimental work of Breedveld *et al.* (1998) who measured long-time diffusivities at high *Pe* and found adequate agreement with previous measurements despite the fact that their mean-square displacement data are limited to times less than $0.6\dot{\gamma}^{-1}$ (cf. figure 14).

Finally, in the Brownian Dynamics system at high *Pe* and at very long times (strain of $O(20)$ and $Pe > 100$ for $\phi = 0.45$) the suspension orders into a string phase (Heyes & Melrose 1993; Rastogi 1995; Foss & Brady 1999), with the strings aligned in the flow direction. In the string phase, the diffusivities are dramatically reduced over what they are in a disordered phase. While it is of interest to study the diffusivities in the string phase (Foss & Brady 1999), here we wish to compare the Stokesian and Brownian Dynamics systems, and the Stokesian Dynamics system with hydrodynamic interactions remains disordered for all *Pe*. As seen in figure 1, meaningful long-time mean-square displacements can be obtained for suspensions without hydrodynamic interactions for strains of $O(1)$ where the suspension is still disordered.

In the absence of hydrodynamic interactions, the rotation of the particles is not coupled with the flow or the microstructure and each particle rotates freely under the influence of rotary Brownian motion exhibiting isotropic rotational self-diffusion governed by the Stokes–Einstein equation, $D_0^{s,r} = kT/8\pi\eta a^3$ for both short and long time scales. Inclusion of hydrodynamic interactions couples rotation and translation resulting in a long-time rotational self-diffusion tensor that varies as a function of ϕ and *Pe*. Calculating this tensor is done in exactly the same manner as the translational self-diffusion tensor except the particle angular displacements are used in lieu of the translational displacements. One notable difference is that the affine angular displacement, $-\frac{1}{2}\dot{\gamma}\hat{\boldsymbol{k}}\Delta t$, is directed along the vorticity axis in simple shear flow and, due to the fact that it has no spatial dependence, does not create any convectively enhanced angular dispersion. For consistency, the affine angular displacements have been subtracted off when calculating the mean-square angular displacements.

4. Results

This work will focus on the equilibrium and non-equilibrium behaviour of the long-time self-diffusivity of a suspension of monodisperse spheres in the presence of Brownian motion with and without hydrodynamic interactions. As discussed earlier, the Péclet number, *Pe*, is the parameter we shall use to determine the relative magnitudes of Brownian motion and the imposed shear flow. The other important parameter of interest in a hard-sphere suspension is the volume fraction, ϕ, which is a measure of the particle concentration. In order to reduce the number of parameters in the system, we limit our study in the following manner: To study the effects of *Pe*, we focus on one volume fraction, $\phi = 0.45$, and vary *Pe* from 0 to 1000 in order to capture the full range of equilibrium and non-equilibrium behaviour. This volume fraction represents a relatively concentrated system, but remains below the equilibrium phase transition at $\phi = 0.494$. Then, to examine the role of the volume fraction, we focus on two Péclet numbers, $Pe = 0$ and $Pe = 1000$, in order to examine the equilibrium and high-shear limits, respectively.

As stated in the previous section, two separate simulation techniques were used in this work. For the Brownian Dynamics simulations, a large system was studied, $N = 1331$, and the number of independent repetitions of each run from different starting configurations was set to be 91. To explain the length of each run, we must discuss the non-dimensionalizations for time in the regimes being studied. At equilibrium and low shear rates ($Pe \leqslant 1$), the diffusive time, a^2/D_0, is used, while at

https://doi.org/10.1017/S0022112099006576 Published online by Cambridge University Press

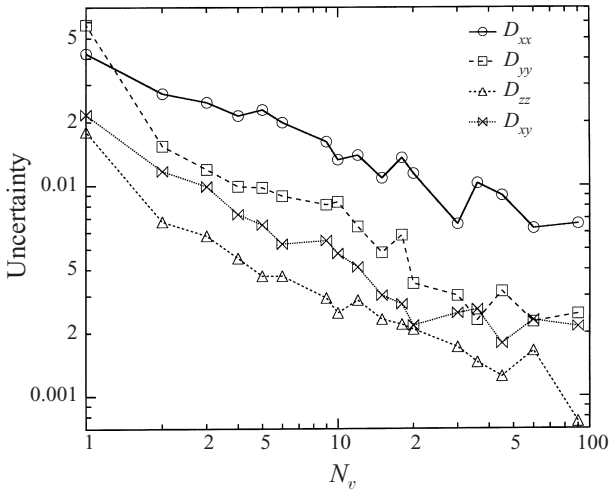

FIGURE 2. Standard deviations calculated from subset averages as a function of the number of data points included in each subset, N_v. These data are from the Stokesian Dynamics system, $\phi = 0.20$, $Pe = 1000$, $N = 27$, and 182 total independent realizations.

high shear rates, the flow time, $\dot{\gamma}^{-1}$, is used. The time step for all the simulations is $\Delta t = 2.5 \times 10^{-4}$ and the number of time steps used is 4000. This sets the length of the simulation to be one particle diffusive time at low shear rates, and one strain at high shear rates. As mentioned before, at high shear rates systems in the absence of hydrodynamics are known to order into strings that are aligned in the flow direction, which results in a significant decrease in the diffusivities. The disorder–order transition generally takes approximately twenty strains to form from an equilibrium starting configuration while the mean-square displacements reach their long-time linear asymptote in less than one strain, as shown in figure 1. Thus, we can extract meaningful long-time self-diffusivities for the disordered state from the limiting behaviour shown in figure 1; specifically, diffusivities were determined from linear fits to the mean-square displacement curves for $0.8 \leqslant \dot{\gamma} t \leqslant 1$.

The Stokesian Dynamics simulations were performed in the same manner but with a few changes. Computational costs limited us to a smaller system, $N = 27$. This was partially compensated for by increasing the number of repetitions to 182. However, for a given run the simulation cell with $N = 27$ is substantially smaller than a cell from a run for Brownian Dynamics with $N = 1331$ and this finite simulation cell may affect the final values for the diffusivities – the results may not give the large-N limit. The same non-dimensionalizations for time are used, but the presence of hydrodynamics has the effect of slowing down the dynamics of the system. For this reason, we used a larger time step of $\Delta t = 5.0 \times 10^{-4}$ while maintaining the total number of steps used at 4000. This sets a longer simulation length of two particle diffusive times near equilibrium, and two strains at high shear rates.

To give the reader an idea of the statistical noise in the results, the following process was performed wherever possible. Each of the 91 (or 182) simulations for each system produces a mean-square displacement curve and a value for the long-time self-diffusivity. These values can then be grouped into subsets of N_v values and averaged. The standard deviation of the subset averages can be used as a measure of the amount of uncertainty in the data. Of course, the measured uncertainty decreases

https://doi.org/10.1017/S0022112099006576 Published online by Cambridge University Press

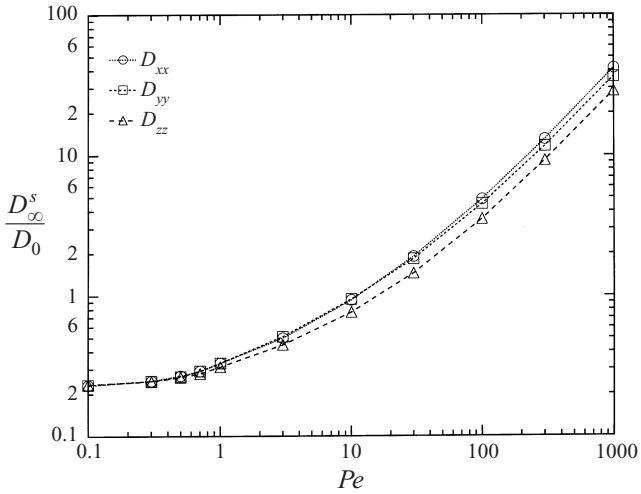

FIGURE 3. Diagonal components of the long-time self-diffusion tensor as a function of Pe for the Brownian Dynamics system. $N = 1331$, $\phi = 0.45$.

as the number of values chosen to be in each subset, N_v, increases. Figure 2 shows the size of the uncertainty as a function of N_v, showing that the error decays like $N_v^{-1/2}$ as one would expect from independent subsets of data. At first, the best choice for N_v would seem to be taking the standard deviation of the diffusivities obtained from each individual simulation, $N_v = 1$. This produces the largest error as the uncertainty in each individual run is determined by the number of particles used and does not take advantage of any averaging over independent realizations and often results in large error bars on data with high internal consistency. In contrast, grouping all of the realizations into one or two subsets might be construed as an attempt to unfairly minimize the uncertainties. We choose an intermediate condition of 6 subsets of 15 (or 30) simulations for use in determining the uncertainty represented by the error bars on our graphs. For the Brownian Dynamics simulations, the error bars are always less than the symbol size and are not shown. No attempt was made to simulate systems with varying N in order to extrapolate for large N because of the large computational cost. This should not be a problem for the Brownian Dynamics system, but the Stokesian Dynamics results may be affected by the small system size used.

4.1. *Shear-rate dependence of diffusivities*

The Pe-dependence of the diagonal components of the long-time self-diffusivity from the Brownian Dynamics simulations are shown in figure 3. The diffusivities tend to their constant isotropic equilibrium values at low Pe, while they grow linearly with Pe, indicating a $\dot{\gamma}a^2$ scaling, at high shear rates. As predicted in § 2, D_{zz} is clearly the smallest of the diagonal components. D_{xx} and D_{yy} are predicted to be roughly equal at high Pe due to a zero first normal stress difference, but the data in figure 3 appear to show that $D_{xx} > D_{yy}$. Figure 4 represents the same data after subtraction of the equilibrium values, clearly showing that the first correction to the diagonal components of the long-time diffusion tensor at small Pe scales as $Pe^{3/2}$ as predicted by theory. The xx- and yy-components are roughly equal at low Pe, both being greater than the zz-component.

Inclusion of hydrodynamic interactions results in similar behaviour. The Pe-dependence of the normal components of the long-time self-diffusivity from the

https://doi.org/10.1017/S0022112099006576 Published online by Cambridge University Press

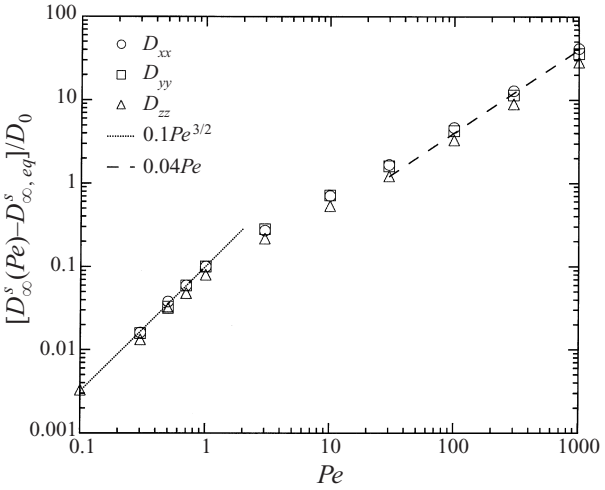

FIGURE 4. Diagonal components of the long-time self-diffusion tensor minus the equilibrium value as a function of *Pe* for the Brownian Dynamics system showing the functional dependence of the first correction of the diffusivity due to the shear flow. $N = 1331$, $\phi = 0.45$.

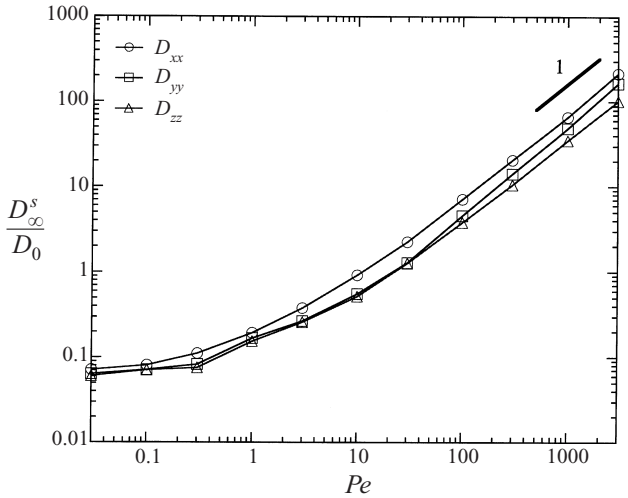

FIGURE 5. Diagonal components of the long-time self-diffusion tensor as a function of *Pe* for the Stokesian Dynamics system. $N = 27$, $\phi = 0.45$.

Stokesian Dynamics simulations are shown in figure 5. Again, the diffusivities approach their isotropic equilibrium values at low *Pe* and grow linearly with *Pe* at high shear rates. The relative size of the normal components at high *Pe* is governed by the same inequality, $D_{xx} > D_{yy} > D_{zz}$, as predicted in § 2. Figure 6 shows the same data after subtraction of the equilibrium diffusivities, showing the enhancement of the normal components of the long-time diffusion tensor by the flow. One can see that the *xx*-component is clearly the largest of the three in agreement with (2), with D_{yy} being slightly larger than D_{zz}. Unfortunately, the $Pe^{3/2}$ scaling predicted in § 2 is not evident. This is most likely due to the fact that the length scale for the convective outer region, $aPe^{-1/2}$, is larger than the box size, $L = a(3/4\pi\phi)^{-1/3}N^{1/3} \approx 6a$, so that the finite-$N$ effects prevent sampling this regime. Also, the characteristic Péclet number

https://doi.org/10.1017/S0022112099006576 Published online by Cambridge University Press

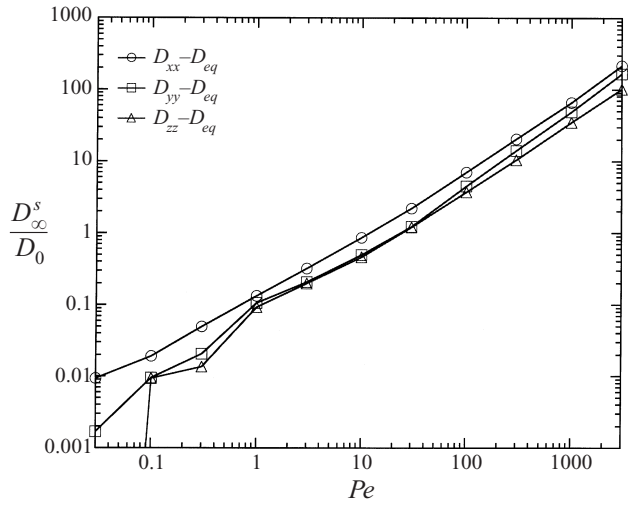

FIGURE 6. Diagonal components of the long-time self-diffusion tensor minus the equilibrium value as a function of Pe for the Stokesian Dynamics system showing the functional dependence of the first correction of the diffusivity due to the shear flow. $N = 27$, $\phi = 0.45$.

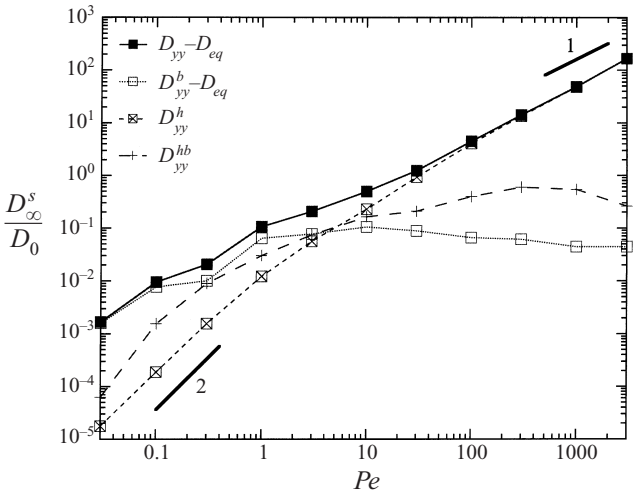

FIGURE 7. The different contributions to the yy-component of the long-time self-diffusion tensor as a function of Pe for the Stokesian Dynamics system. $N = 27$, $\phi = 0.45$. The equilibrium value of the self-diffusivity is subtracted from the Brownian contribution and total diffusivity to focus on the effects of the shear flow.

for systems involving hydrodynamic interactions is $\overline{Pe} = Pe/D^s_0(\phi)$, which necessitates the use of even smaller Pe when examining the near equilibrium behaviour.

It is very interesting to note that the shear-induced diffusivities with and without hydrodynamics at high Péclet number are comparable in magnitude, in agreement with the prediction of Brady & Morris (1997).

The different contributions to the diffusivities with hydrodynamic interactions are examined in figure 7 for the yy-component; the xx- and zz-components behave in the same fashion and are not shown. At equilibrium, only the random Brownian displacements are present and the long-time self-diffusivity is solely defined by its

https://doi.org/10.1017/S0022112099006576 Published online by Cambridge University Press

Brownian contribution, $D^s_{\infty,b}$. Here, it is useful to subtract the equilibrium value from the Brownian contribution in order to study the effects of the flow on diffusion: $D^s_{\infty,b} - D^s_{\infty,eq}$ represents the enhancement of the random-walk-type diffusion due to the presence of the imposed flow. At low *Pe* the main enhancement of the diffusivity is from $D^s_{\infty,b}$, which indicates that the first correction is due to random-walk-type diffusion that is facilitated by the external flow. We propose the following mechanism for the enhancement of the Brownian contribution to the diffusivity. Imagine the particles in the suspension occupying sites on a lattice. In a Brownian random walk a particle moves from one site to a neighbouring unoccupied site. In the dilute limit, the particle is free to step in any direction at any time because none of the other sites are occupied. As the concentration is increased, the chances of a neighbouring site being occupied increase, reducing the ability of a particle to make a step. The number of occupied neighbour sites is not a constant with time as all particles are undergoing the same random-walk process producing local density fluctuations. A particle diffusing over long distances in a dense suspension will often be trapped in a region of high density and be forced to wait until that fluctuation dissipates, resulting in a low value of the diffusivity. Now, apply a shear flow to the lattice. Particles are still confined to the lattice sites, but these sites are convected along with the flow. All motion in the velocity-gradient direction is still caused by the random walk, but the neighbouring sites are changing with time due to the shear flow. The effect of this is that a high density fluctuation hindering the motion of a tagged particle can – in addition to dissipating as a result of random-walk-type diffusion – be convected away from the tagged particle enabling random-walk motion in the velocity-gradient direction. This results in a larger value of $D^s_{\infty,b}$ relative to that at equilibrium. Note that $D^s_{\infty,b}$ is never greater than its dilute-limit value, D_0, as the easiest random walk is one in the absence of any other particles. The shearing motion simply lessens the hindering effects of neighbouring particles on random-walk diffusion. This effect increases as the shear rate increases and ultimately saturates. At high *Pe* particles are driven into near contact by the shearing motion and the lubrication forces reduce the particle mobility, or short-time self-diffusivity. At smaller *Pe*, the reduction is rather small, but for $Pe > 10$ this clustering intensifies, the hydrodynamic viscosity increases and the drop in particle mobility becomes quite significant resulting in smaller random displacements and a decrease in $D^s_{\infty,b}$. Indeed, our results show that $D^s_{\infty,b}$ reaches a maximum at $Pe \approx 10$ where the effects of decreased mobility begin to cancel the effects of the enhanced random walk in a shearing microstructure.

The hydrodynamic diffusivity $D^s_{\infty,h}$, also shown in figure 7, is the dominant contribution at high *Pe* and grows linearly with *Pe*, or in dimensional form as $\dot{\gamma}a^2$, the shear-induced diffusivity scaling. At low *Pe*, this contribution is very small, apparently vanishing as Pe^2 as the figure shows. The behaviour of the hydrodynamic diffusivity can be explained by noting that the diffusion constant can be defined as a time integral of the velocity autocorrelation function. Fluctuations in the hydrodynamic velocity scale like $\dot{\gamma}a$; thus, the velocity autocorrelation scales as $\dot{\gamma}^2a^2$. Near equilibrium the correlation time for the velocity fluctuation is the diffusive time, a^2/D_0, resulting in an $O(D_0Pe^2)$ hydrodynamic contribution. At high shear rates, the correlation time is the flow time $\dot{\gamma}^{-1}$, giving a hydrodynamic diffusivity of $O(D_0Pe)$. It should be noted that the behaviour at high *Pe* may be qualitatively different from the behaviour in the pure hydrodynamic limit ($Pe^{-1} \equiv 0$). The pure hydrodynamic limit may exhibit no self-diffusion due to symmetry properties present in the low-Reynolds-number microstructure. It is not known at this time whether the pure-hydrodynamic limit has chaotic particle trajectories that generate a truly diffusive motion. It is known,

https://doi.org/10.1017/S0022112099006576 Published online by Cambridge University Press

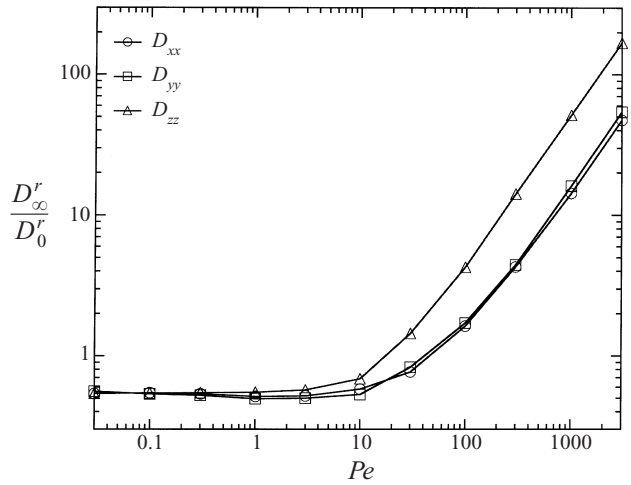

FIGURE 8. Diagonal components of the rotational long-time self-diffusion tensor as a function of Pe for the Stokesian Dynamics system. $N = 27$, $\phi = 0.45$.

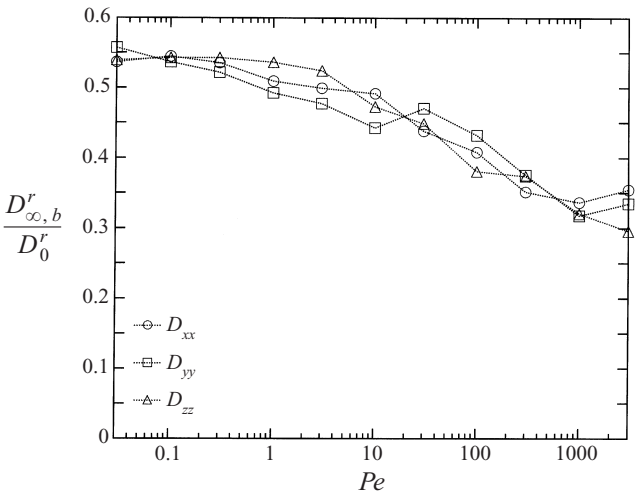

FIGURE 9. Brownian contribution to the diagonal components of the rotational long-time self-diffusion tensor as a function of Pe for the Stokesian Dynamics system. $N = 27$, $\phi = 0.45$.

however, that at high volume fractions the suspension jams up and ceases to flow (Melrose & Ball 1995), so the question of diffusion may be moot. At finite Pe the Brownian displacements do more than produce $D^s_{\infty,b}$ which, by itself, is a negligible part of the total diffusivity; they prevent the jamming and break the symmetry producing a microstructure suitable for hydrodynamic diffusion to occur.

The cross-correlation between the hydrodynamic and Brownian displacements, $D^s_{\infty,hb}$, is also shown in figure 7. It is slightly less than the geometric mean of $D^s_{\infty,b}$ and $D^s_{\infty,h}$ at intermediate Péclet numbers indicating a strong cross-correlation and less at extreme values of Pe. It is important to note that $D^s_{\infty,hb}$ is greater than zero for all Pe indicating that the total diffusivity is always greater than the sum of the Brownian and hydrodynamic contributions, and that at no point are the two displacements negatively correlated and act against each other.

https://doi.org/10.1017/S0022112099006576 Published online by Cambridge University Press

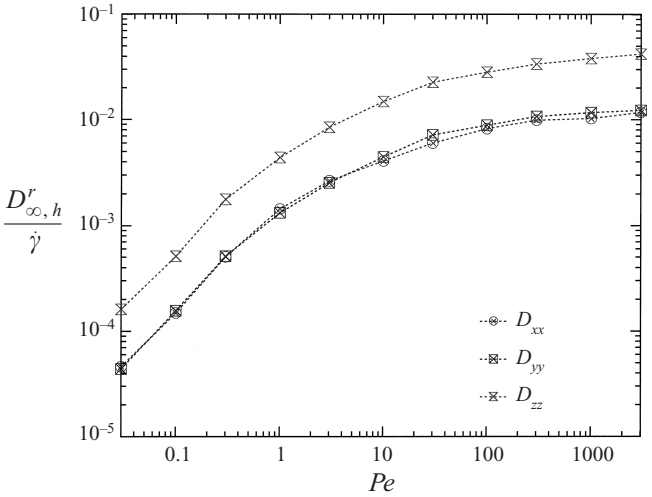

FIGURE 10. Hydrodynamic contribution to the diagonal components of the rotational long-time self-diffusion tensor, non-dimensionalized by the appropriate hydrodynamic scaling, $\dot\gamma$, as a function of *Pe* for the Stokesian Dynamics system. $N = 27$, $\phi = 0.45$.

Results for the diagonal components of the rotational long-time self-diffusion tensor with hydrodynamics are shown in figure 8. As is the case with the translational analogues, the rotational diffusivities, when non-dimensionalized by the Stokes–Einstein rotational diffusion coefficient, $D_0^{s,r}$, approach their constant equilibrium value at low *Pe* and grow linearly, indicating a $\dot\gamma$ scaling, at high shear rates. The largest of the three diagonal components is D_{zz} for the entire range of *Pe*. The difference is small near equilibrium as the suspension microstructure is close to isotropic, and quite large at high *Pe* where the *zz*-component is over three times greater than the other two components as this is the direction of the affine angular displacements. One intriguing difference in the rotational diffusivities as compared to their translational counterparts is that there is a slight decrease in the diffusivity with *Pe* at low *Pe*. Figure 9 for the Brownian contribution to the diffusivity shows that $D^{s,r}_{\infty,b}$ clearly has its maximum at equilibrium and there is no evidence of any enhancement of 'random-spin-type' diffusion in non-equilibrium configurations. The hydrodynamic contribution to the diffusivities in figure 10 is scaled by $\dot\gamma$ showing linear growth (Pe^2 growth when scaled by $D_0^{s,r}$) at low *Pe*, and approaching a constant at high *Pe* quite similar to the translational counterparts. The transition from low-shear to high-shear behaviour occurs at higher *Pe* for the rotational diffusivities. The $D^{s,r}_{\infty,hb}$ contribution (not shown) to the diffusivity is small for all *Pe* indicating little correlation between the hydrodynamic and Brownian angular displacements.

4.2. *Volume-fraction dependence of the diffusivities*

We now turn our discussion to the effects of volume fraction ϕ on the high- and low-*Pe* limits of the diagonal components of the long-time self-diffusion tensor. At $Pe = 0$, the suspension is isotropic and all the diagonal components are equal; thus, all the components can be averaged together tripling the amount of data and decreasing the amount of noise present in the results. Figure 11 shows the long-time diffusivity at equilibrium as a function of ϕ with and without hydrodynamics. Also shown in the figure are previous simulation results of hard spheres in the absence of hydrodynamic interactions. Schaertl & Sillescu (1994) employed the same simulation

https://doi.org/10.1017/S0022112099006576 Published online by Cambridge University Press

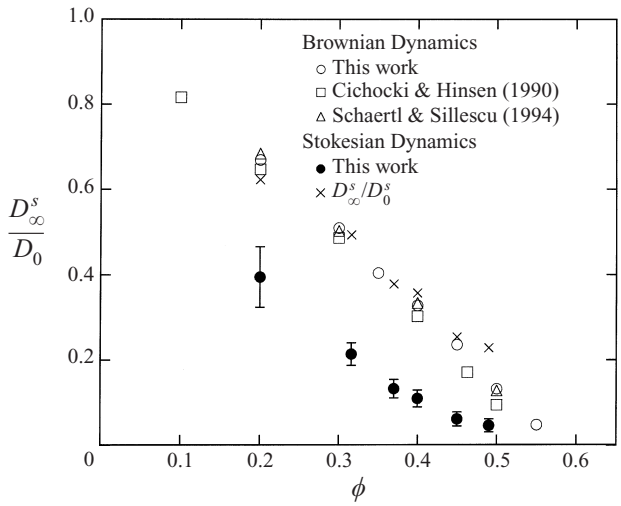

FIGURE 11. Equilibrium values of the long-time self-diffusivity as a function of ϕ. Data include those from both the Brownian Dynamics and Stokesian Dynamics systems along with previous Brownian Dynamics results. Also plotted are the Stokesian Dynamics data after division by the equilibrium short-time self-diffusivities as suggested by Brady (1994).

method used in this work and studied only the equilibrium behaviour. This method allows for some particle overlap due to a finite-size time step and thus exhibits a diffusivity that may be slightly larger than the true hard-sphere value. Cichocki & Hinsen (1992) used a method in which particles take small random steps and if an overlap occurs, the steps leading to the overlap are rejected and another random step is chosen. This method should produce a diffusivity slightly smaller than the true hard-sphere diffusivity. Nonetheless, the three sets of data are in good agreement with each other suggesting that errors due to finite-size time steps are small. The diffusivity with hydrodynamics is smaller due to the decrease in the short-time diffusivity from a reduced particle mobility which decreases the size of the random Brownian steps. The mode of diffusion at equilibrium is of random-walk type, which is hindered by the presence of other particles, causing the diffusion constant to decrease monotonically as ϕ is increased. Indeed, Brady (1994) showed that the long-time self-diffusivities with and without hydrodynamics are simply related by the hydrodynamically-determined short-time self-diffusion coefficient: $(D^s_\infty)_{hydro} = D^s_0(\phi)(D^s_\infty)_{nohydro}$; the data in figure 11 agree with this scaling behaviour. Brady (1994) showed that Stokesian Dynamics results for D^s_∞ agree very well with experimental data.

Rotational self-diffusivities are plotted in figure 12 along with their short-time counterparts, which are simply the particles' average instantaneous hydrodynamic rotational mobility. Unlike translational diffusion, there is no hindrance to rotational diffusion without the presence of hydrodynamic lubrication forces, which are also less singular at contact than their translational lubrication counterparts. This results in rotational self-diffusivities that are much larger in comparison to their translational counterparts. Also, the long-time rotational diffusivities are only slightly less than their short-time counterparts indicating that the dynamic microstructure plays only a small role in the diffusive behaviour. The experimental results of Digiorgio *et al.* (1995) for the rotational short-time self-diffusivities are also included in figure 12 for comparison with the simulation data. There are no corresponding results for Brownian Dynamics simulation because in the absence of hydrodynamic interactions particle

https://doi.org/10.1017/S0022112099006576 Published online by Cambridge University Press

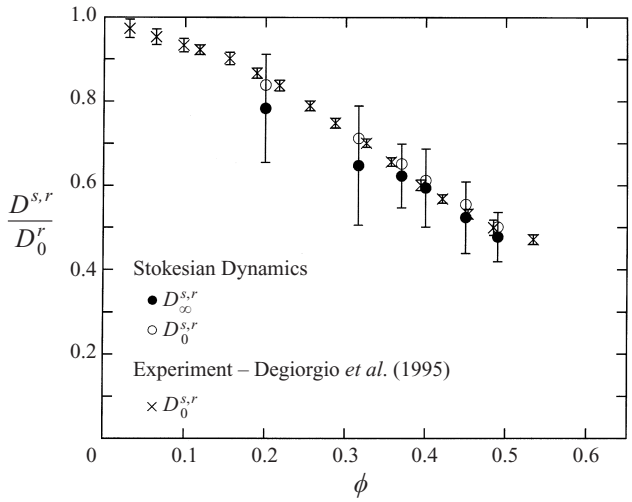

FIGURE 12. Equilibrium values of the rotational long-time self-diffusivity as a function of ϕ for the Stokesian Dynamics system. Values of the rotational short-time diffusivity from both simulation and experiment are included for comparison.

rotational mobility is unity and unaffected by the dynamics of the microstructure, and the long- and short-time rotational self-diffusivities are equal to each other and equal to the dilute limit Stokes–Einstein diffusivity $D_0^{s,r}$.

At high *Pe*, the mechanisms for diffusion are markedly different from those at equilibrium. Diffusion is driven by particle–particle interactions that prevent coincident particles on neighbouring streamlines in shear flow from passing through one another. The frequency of these interactions increases with volume fraction. Simulation data are not available at dilute volume fractions as particle collisions are so infrequent that the mean-square displacements do not reach their long-time asymptote in the time of the simulation runs. In the dilute limit it may be more fruitful to employ the trajectory calculation scheme of da Cunha & Hinch (1996).

The normal components of $\boldsymbol{D}_\infty^s$ at $Pe = 1000$, scaled by $\dot{\gamma}a^2$, the appropriate scale for high-*Pe* diffusion, are shown for the Brownian Dynamics system in figure 13(*a*) and the Stokesian Dynamics system in figure 13(*b*). For the Brownian Dynamics system, all three diffusivities are monotonic increasing functions of ϕ; D_{zz} is clearly the smallest of the three diffusivities with D_{xx} slightly greater than D_{yy} for all except for the highest volume fraction where D_{yy} is larger. The Stokesian Dynamics results show somewhat different behaviour. The inequality $D_{xx} > D_{yy} > D_{zz}$ holds for all ϕ, but only D_{zz} clearly appears to be monotonically increasing in this range of ϕ. Of the other terms, D_{yy} increases at first and reaches a plateau, and D_{xx} appears to be constant over the entire range studied here. This differs from the Brownian Dynamics result and is not in agreement with the theoretical results of Brady & Morris (1997) who predict that all components are strictly increasing functions of ϕ, with and without hydrodynamic interactions. Due to system size constraints, we were not able to study larger and more dense systems to validate these behaviours. A possible reason for the non-monotonic growth is that for the Stokesian Dynamics system the characteristic Péclet number is $\overline{Pe} = Pe/D_0^s(\phi)$, and since D_0^s is a monotonically decreasing function of ϕ, $Pe = 1000$ represents a different $\overline{Pe}$ for each value of ϕ. A more accurate study would be to fix $\overline{Pe}$, which would involve knowing D_0^s *a priori*.

https://doi.org/10.1017/S0022112099006576 Published online by Cambridge University Press

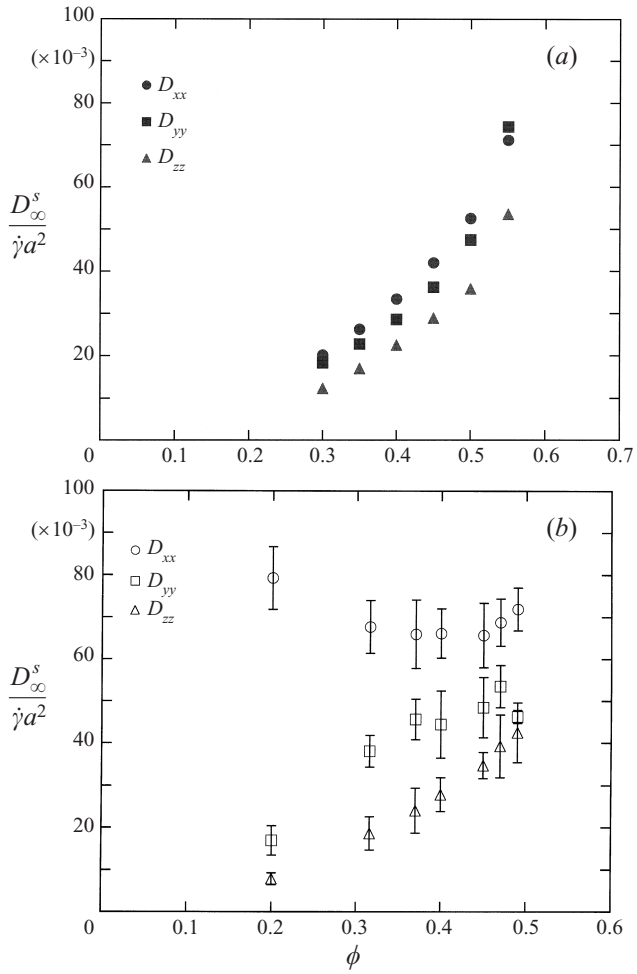

FIGURE 13. High shear values of the long-time self-diffusion tensor, non-dimensionalized by $\dot{\gamma}a^2$, for (*a*) the Brownian Dynamics system and (*b*) the Stokesian Dynamics system. The high shear points here correspond to $Pe = 1000$.

Also, it is not known for perfect hard spheres with hydrodynamics as $Pe \to \infty$ if the motion is diffusive, and this may be affecting the behaviour for large Pe in figure 14. The high shear values of the yy- and zz-components of the long-time self-diffusion tensor are compared with the experimental data of Eckstein, Bailey & Shapiro (1977), Leighton & Acrivos (1987), Phan & Leighton (1993) and Breedveld *et al.* (1998) and the theoretical estimates of Brady & Morris (1997) in figures 14(*a*) and 14(*b*), respectively.

Brady & Morris (1997) use a boundary layer analysis to predict that the shear-induced long-time self-diffusivity in the absence of hydrodynamic interactions scales as

$$D^s_\infty \sim \dot{\gamma}a^2\phi g^\infty(\phi), \tag{13}$$

where $g^\infty(\phi)$ is the pair-distribution function at infinite Pe as particle–particle contact is approached from outside the boundary layer. Hydrodynamic interactions change

https://doi.org/10.1017/S0022112099006576 Published online by Cambridge University Press

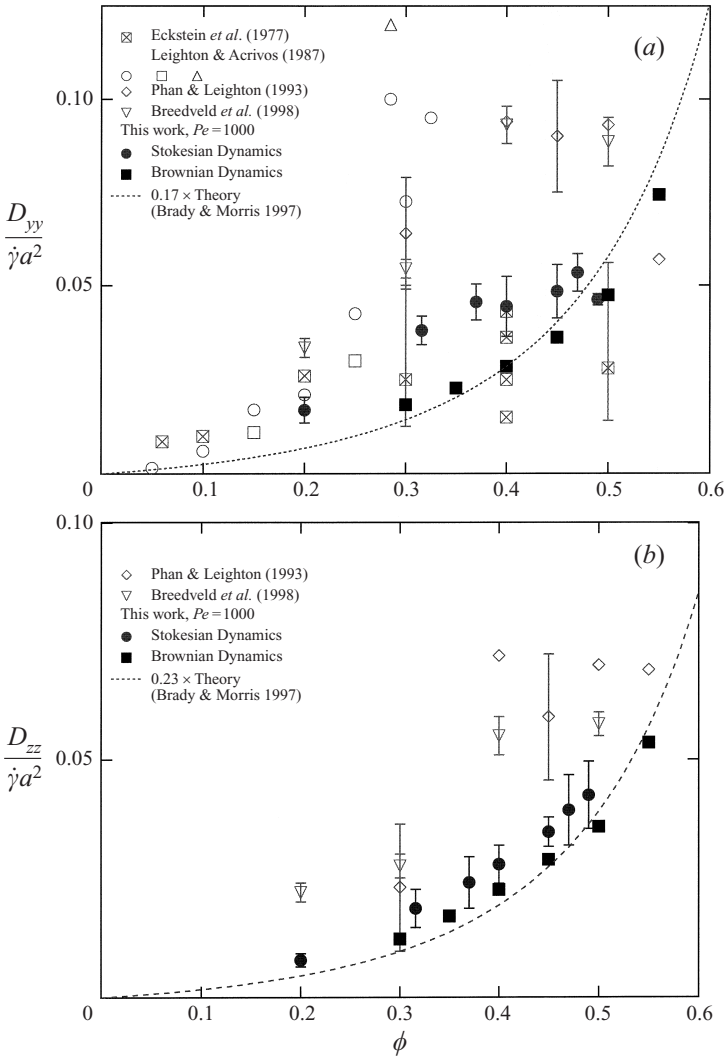

FIGURE 14. Comparison of the high shear (*a*) *yy*-components and (*b*) *zz*-components of the long-time self-diffusion tensor from the Stokesian Dynamics and Brownian Dynamics systems with previous experimental results.

the scaling to

$$D^s_\infty \sim \dot{\gamma}a^2(b/a-1)^{0.22}\phi g^\infty(\phi), \tag{14}$$

where the particles interact through a hard-sphere repulsive force at a radius $b > a$, where a is the hydrodynamic radius. The functions $g^\infty(\phi)$ have the same physical significance in (14) and (13), although the numerical value may be different with and without hydrodynamics. Note that in the pure hydrodynamic limit of no interparticle forces $b \to a$ and the diffusivity is zero. That is why our simulation results are reported for large but finite *Pe*, as the residual Brownian motion breaks the flow reversal symmetry and allows diffusion.

The theory does not predict $g^\infty(\phi)$ nor the coefficient in front. In the dilute limit $g^\infty(\phi) \to 1$ and in the absence of hydrodynamic interactions numerical coefficients are

https://doi.org/10.1017/S0022112099006576 Published online by Cambridge University Press

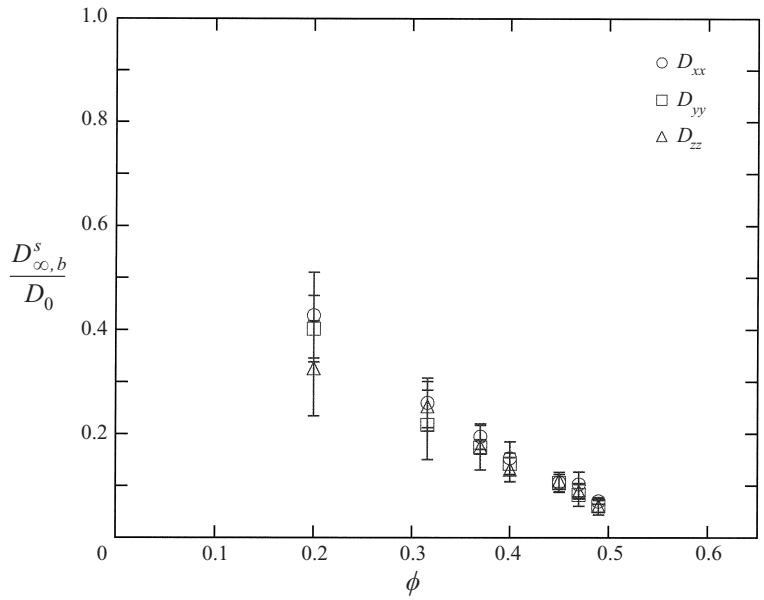

FIGURE 15. Brownian contribution to the high shear values of the long-time self-diffusion tensor for the Stokesian Dynamics system. The high shear points here correspond to $Pe = 1000$.

given in Brady & Morris (1997). Since $g^{\infty}(\phi)$ is not known theoretically, in figure 14 we have used the equilibrium pair-distribution function at contact $g^0(\phi)$ for hard spheres determined from the Carnahan–Starling equation of state. This should be a reasonable estimate for the ϕ-dependence of $g^{\infty}(\phi)$ over the volume-fraction range studied here. The numerical coefficients reported were simply fit to the data, i.e.

$$D_{yy} = 0.23\frac{16}{45\pi}\dot{\gamma}a^2\phi g^0(\phi), \qquad D_{zz} = 0.17\frac{8}{45\pi}\dot{\gamma}a^2\phi g^0(\phi),$$

were used, where the factors $\frac{16}{45}\pi$ and $\frac{8}{45}\pi$ are the dilute-limit predictions of Brady & Morris (1997).

Note that the shear-induced diffusivities with and without hydrodynamics are of roughly the same magnitude, in keeping with the above theory of Brady & Morris (1997).

Although the Stokesian Dynamics diffusivity at high Pe is dominated by its hydrodynamic contribution, there is a small Brownian contribution that scales like D_0 and is shown in figure 15. This contribution is a monotonically decreasing function of ϕ, exhibiting the same qualitative behaviour at both high and low Pe, as random walks are always hindered by the presence of other particles. The magnitudes are the same as at equilibrium.

Rotational self-diffusivities are shown in figure 16. Again, there appears to be an increase in the values of the diffusivity at lower ϕ, which reaches a plateau at higher ϕ. The zz-component is by far the largest of the three diagonal components, with $D_{yy} > D_{xx}$ at the lower volume fractions and those two components being roughly equal at higher ϕ. Rotational diffusion is dominated by its hydrodynamic contribution at high Pe. The Brownian contributions in figure 17 show similar magnitudes and behaviour to the equilibrium rotational diffusivities as Brownian diffusion is hindered as the concentration is increased.

https://doi.org/10.1017/S0022112099006576 Published online by Cambridge University Press

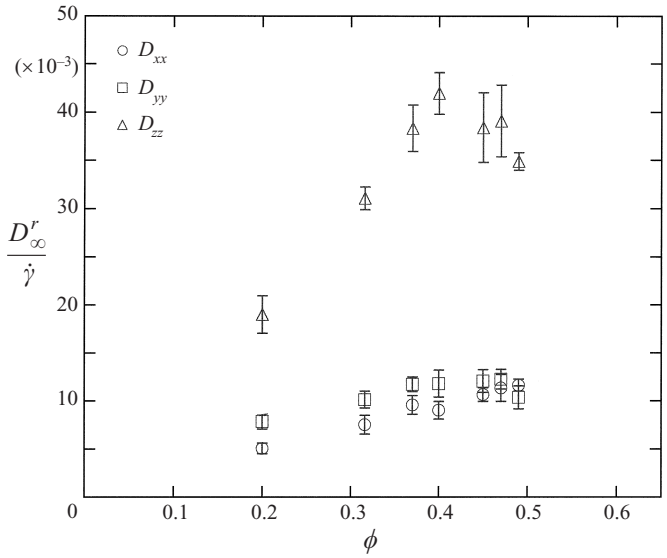

FIGURE 16. High shear values of the rotational long-time self-diffusion tensor, nondimensionalized by $\dot\gamma$, for the Stokesian Dynamics system. The high shear points here correspond to $Pe = 1000$.

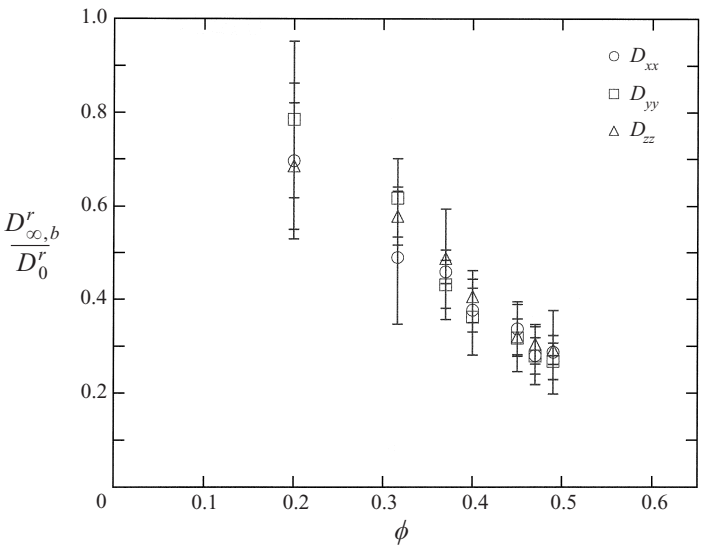

FIGURE 17. Brownian contribution to the high shear values of the rotational long-time self-diffusion tensor for the Stokesian Dynamics system. The high shear points here correspond to $Pe = 1000$.

5. Off-diagonal components of the self-diffusion tensor

The long-time self-diffusion tensor, being symmetric, has six independent components. The three diagonal components have been discussed in the previous section. Of the three off-diagonal components all are zero with the exception of $D_{xy} = D_{yx}$ for both translational and rotational diffusion in simple shear flow. Here, we shall discuss the results for this interesting component and also possible physical mechanisms for off-diagonal diffusion.

The diagonal components of $\boldsymbol{D}^s_\infty$ are straightforward to interpret in terms of the

https://doi.org/10.1017/S0022112099006576 Published online by Cambridge University Press

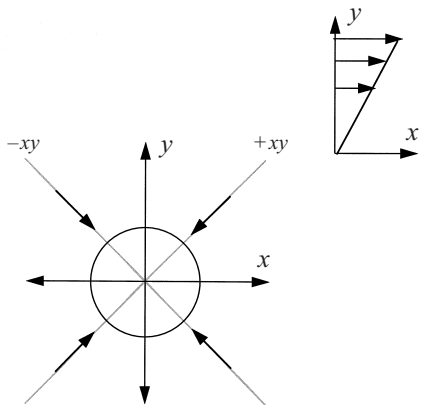

FIGURE 18. The (x, y)-plane in simple shear flow with one particle at the origin. Arrows show impact on the motion of the centre particle due to collisions with other particles.

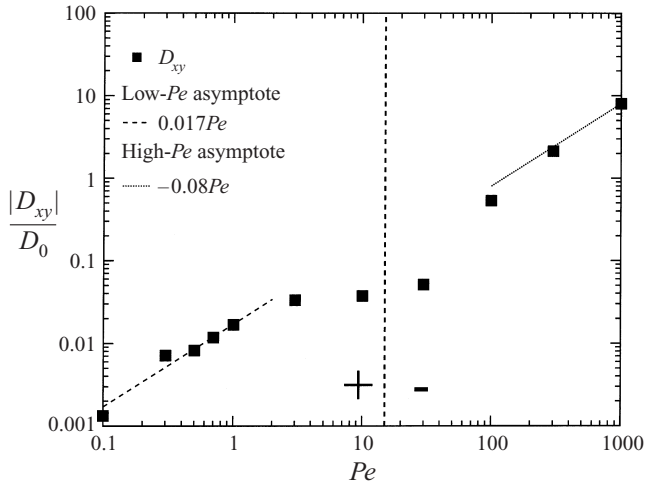

FIGURE 19. The xy-values of the long-time self-diffusion tensor as a function of Pe for the Brownian Dynamics system. $N = 1131$, $\phi = 0.45$.

macroscopic flux of tagged particles given by Fick's law: D_{xx} represents a particle's ability to diffuse in the x-direction and so forth. To understand the D_{xy} component requires examination of its corresponding mean-square displacement, $\langle x(t)y(t)\rangle$. As shown in figure 18, the positive and negative xy-axes correspond to the extensional and compressional directions in shear flow, respectively. Motion in the extensional direction, whether it be outward or inward, results in positive xy-displacements and diffusivities. Similarly, motion in the compressional direction results in negative xy-displacements and diffusivities. Therefore, the sign and magnitude of D_{xy} show which direction is more conducive to diffusion and by how much.

The Pe-dependence of D_{xy} at $\phi = 0.45$ in the absence of hydrodynamic interactions is shown in figure 19. At low shear rates, the diffusivity is positive and grows linearly with Pe. The diffusivity reaches a maximum at $Pe \approx 10$ followed by an abrupt decrease and sign change. At high Pe, D_{xy} is negative and its absolute value grows linearly with Pe. All of this behaviour is in agreement with the theoretical predictions of Morris & Brady (1996) and Brady & Morris (1997).

https://doi.org/10.1017/S0022112099006576 Published online by Cambridge University Press

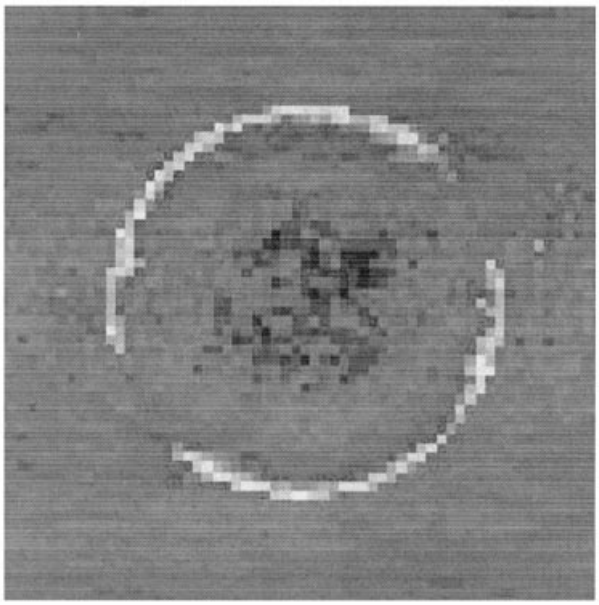

FIGURE 20. Projection of the pair-distribution function onto the (x, y)-plane obtained from Stokesian Dynamics simulation, $\phi = 0.45$, $Pe = 1000$. High probability is represented by light shades, low probability by dark shades. Note the thin arcs of high probability near contact in each compressional zone characteristic of the boundary layer.

According to (1), at low Pe the first correction to the diffusivity is $O(Pe\hat{\boldsymbol{E}})$, resulting in a D_{xy} that grows linearly with Pe. Morris & Brady (1996) show two contributions to this term. The first comes from random-walk, equilibrium-type diffusion occurring in the $O(Pe\hat{\boldsymbol{E}})$ deformed microstructure first calculated by Batchelor (1977). The pair probability, and therefore effectively the volume fraction, in the compressional zones is higher than in the extensional zones due the perturbation of the structure by the flow. Since long-time self-diffusion at equilibrium is a strictly decreasing function of volume fraction, there is greater diffusion along the extensional axis than the compressional axis, resulting in a positive D_{xy}. The second contribution involves examining the $O(Pe)$ effects of the flow on the diffusion process in an equilibrium microstructure (denoted by the function $\boldsymbol{b}_1$ in Morris & Brady 1996). Motion of a tagged particle in the compressional direction will increase the probability that a particle–particle collision, which hinders random-walk-type diffusion, will take place due to the relative motion of the other particles in the shear flow. Conversely, particles in the extensional zone are being convected away from a marked particle and motion along the extensional axis is less likely to result in a particle–particle collision. This facilitates motion in the extensional direction compared to the compressional direction. Thus, each process scales as Pe and each results in a positive contribution to D_{xy}.

The behaviour of D_{xy} at high shear rates in the absence of hydrodynamic interactions can be explained by the relationship between diffusion and stress given in (3). In contrast to the behaviour at low shear rates where particle–particle collisions are a hindrance to random walks, collisions are the principal mechanism producing diffusion at high Pe. The arrows in figure 18 show the effects of these collisions on the motion of the test particle in the centre of the figure. There is a high probability of particles near contact in the compressional zone at high shear rates (Brady & Morris

https://doi.org/10.1017/S0022112099006576 Published online by Cambridge University Press

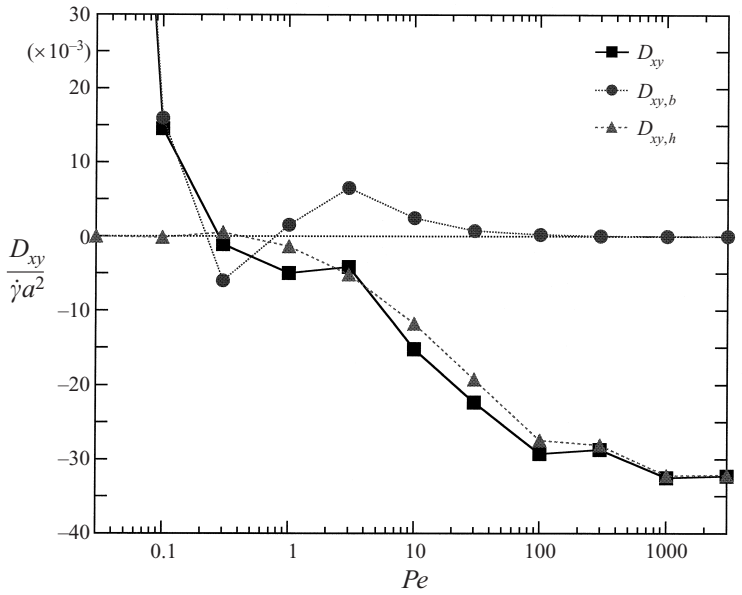

FIGURE 21. The xy-values of the long-time self-diffusion tensor and their different contributions as a function of Pe for the Stokesian Dynamics system. $N = 27$, $\phi = 0.45$.

1997), as shown by our simulations in figure 20. This high probability density in a boundary layer at contact is the origin of the $O(\eta\dot{\gamma})$ stresses seen in these systems and increases the number of collisions – and therefore the particle motion – along the compressional axis, resulting in a negative value of D_{xy}. Inclusion of hydrodynamic interactions produces qualitatively similar behaviour.

Figure 21 shows D_{xy} and its main contributions as a function of Pe for the Stokesian Dynamics system. As with the diagonal components, the data are best at higher Pe where negative diffusivities of magnitude $\dot{\gamma}a^2$ are clearly seen, in agreement with the theoretical work of Brady & Morris (1997). Near equilibrium, where D_{xy} is predicted to vanish linearly with Pe, the small Stokesian Dynamics system proves unable to resolve the behaviour. What is clear from the data, however, is that D_{xy} is indeed positive and dominated by the Brownian contribution, validating the mechanism proposed above.

The collective or Fickian diffusion coefficient measures a particle's ability to diffuse down a concentration gradient and is determined from Fick's law,

$$\boldsymbol{j} = -\boldsymbol{D}^c \cdot \nabla n, \tag{15}$$

where $\boldsymbol{j}$ is the particle flux and n is the particle concentration. Self-diffusion, which we have studied here, corresponds to the Fickian flux of a tracer or tagged particle as it diffuses down its (weak) concentration gradient. From this perspective of flux down a concentration gradient, what do off-diagonal terms in the diffusion tensor mean? Can a gradient in one direction cause a flux in another? To analyse this, we shall look at high-Pe simple shear flow with a concentration gradient in either the x- or y-directions.

A positive concentration gradient in the x-direction is illustrated in figure 22(a). At large Pe, the diffusive motion of particles is driven by the formation of particle doublets that exhibit solid-body-like clockwise rotation with the vorticity of the simple

https://doi.org/10.1017/S0022112099006576 Published online by Cambridge University Press

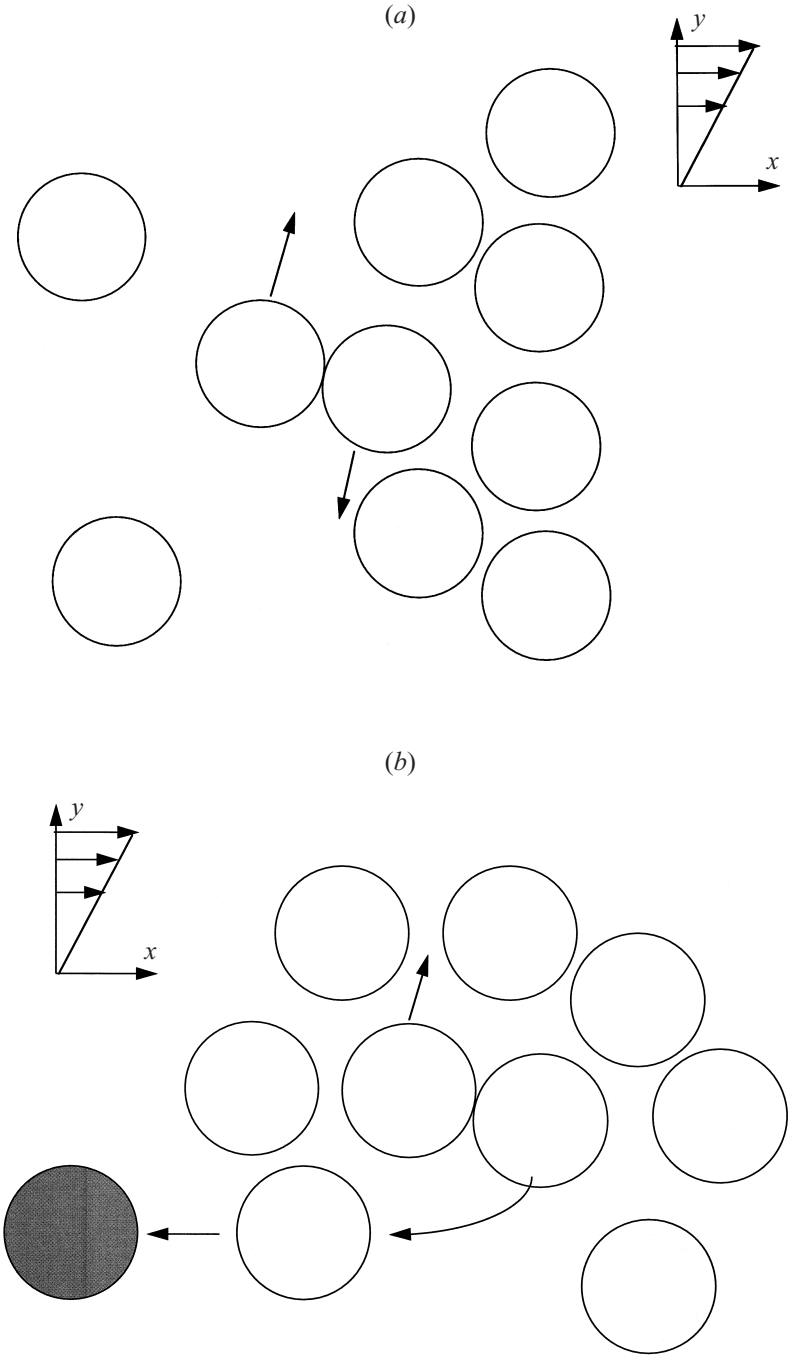

FIGURE 22. (*a*) Configuration of particles with a concentration gradient in the positive x-direction showing a possible mechanism for a flux in the positive y-direction. (*b*) Configuration of particles with a concentration gradient in the positive y-direction showing a possible mechanism for a flux in the positive x-direction. Note that the darker particle shows where the particle would have been if it had precisely followed its affine x-displacements. Although the particle is convected to the left by the flow, there is a lag which is indicative of a positive x-flux.

https://doi.org/10.1017/S0022112099006576 Published online by Cambridge University Press

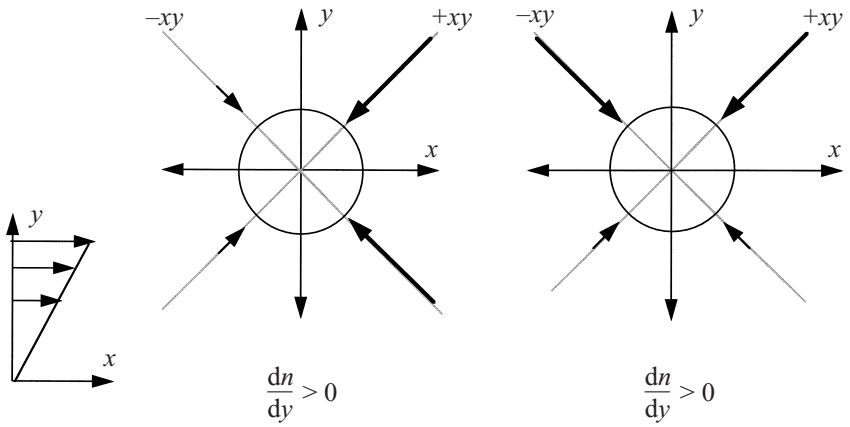

FIGURE 23. The (x, y)-plane in simple shear flow with one particle at the origin. Arrows showing impact on the motion of the centre particle due to collisions with other particles are altered by the presence of a concentration gradient. Larger and darker arrows are drawn on the side with higher concentration due to an increase in the number of collisions in this region.

shear flow. In the absence of lubrication interactions, these doublets do not form and the suspension orders (Bossis & Brady 1984; Dratler, Schowalter & Hoffman 1997). (Note we have specifically limited the Brownian Dynamics simulations to times before ordering to probe the diffusive behaviour in the disordered microstructure.) For the doublet in figure 22(*a*), the particle on the left is in a region of lower concentration and therefore rotates more easily than the particle to its right. The net result is a flux of particles in the positive y-direction, and from (15) a negative D_{yx}.

The other case of a positive concentration gradient in the y-direction is shown in figure 22(*b*). Here, the particle on the right is 'freer' to rotate because it is moving into a region of lower concentration, causing a flux downward into a leftward-moving streamline. At first glance this would appear to result in flux in the negative x-direction, but when the affine motion is taken into account, this is not the case. As the doublet is rotating downward, the leftward motion of the particle on the right is impeded by the presence of the other particle in its compressional zone. This causes a 'lag' in the particle's leftward motion resulting in a net flux in the positive x-direction. To show this more explicitly, one can take the time-dependent positions of the particle, $(x(t), y(t))$, and calculate the affine displacements along the path to calculate the affine contribution:

$$\boldsymbol{x}_a(t) = \int \dot{\gamma} y(t)\, \mathrm{d}t.$$

Since the particle is hindered by its contacting neighbour on the compressional axis, the actual x-displacement is less than the affine displacement resulting in a net positive x-displacement. From Fick's law (15) we have $D_{xy} < 0$.

This gradient or Fickian diffusion can also be approached by looking at relative displacements of particles in the different quadrants of the (x, y)-plane. Figure 23 is similar to figure 18 except that the arrows have been made longer and darker on the side of the test particle with higher concentration. This is done intuitively on the basis that the higher concentration of particles causes a larger impact on the test particle in the centre of the figure due to a relative increase in the number of particle–particle collisions in these regions compared to the regions of lower concentration. Noting

https://doi.org/10.1017/S0022112099006576 Published online by Cambridge University Press

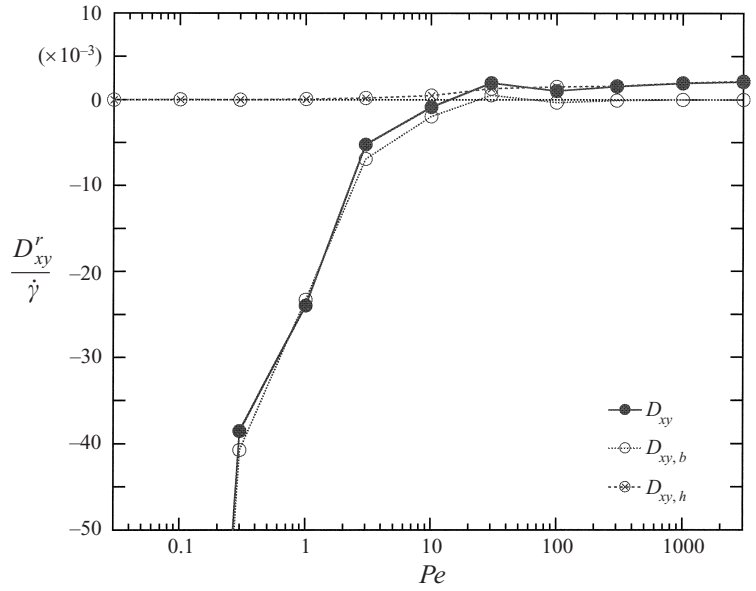

FIGURE 24. The xy-values of the rotational long-time self-diffusion tensor and their different contributions as a function of Pe for the Stokesian Dynamics system. $N = 27$, $\phi = 0.45$.

again the boundary layer in the compressional zones in figure 20, one can see the positive y- and x-fluxes that will result from positive x- and y-gradients, respectively.

The long-time rotational self-diffusivity also has a non-zero off-diagonal component, D^r_{xy}, in the presence of hydrodynamic interactions. Values of D^r_{xy} as a function of Pe in figure 24 show behaviour that is quite similar to the translational case except that each contribution has the opposite sign. At high Pe, the hydrodynamic contribution dominates showing a positive contribution that grows linearly with Pe. Near equilibrium, the negative Brownian contribution dominates but the numerical data are too noisy to obtain a definitive low-Pe asymptote.

The mechanisms for off-diagonal rotational diffusion are related to those of the translational case in that they are dependent on a higher probability of a tagged particle having a neighbour in the compressional, rather than the extensional, zones. Consider first the near equilibrium case where Brownian motion dominates. For two particles near contact with each other, the ability to rotate is easiest along an axis of rotation coincident with the centre-to-centre vector between the particles and is most hindered along any direction perpendicular to this vector. In a shearing suspension, there is a surplus of particles in the compressional zones, thus the favoured axis for rotational diffusion is the compressional axis, while unfavoured axes lie in the extensional–vorticity plane. The preference for rotation along the compressional rather than extensional axis results in a negative Brownian contribution to D^r_{xy}.

At high Pe, the hydrodynamic contribution dominates. Hydrodynamic rotations are caused by a rolling motion that neighbouring particles exhibit as they are convecting past each other in the flow. Most of the rotation occurs in the plane of shear, explaining the much larger values of D^r_{zz} compared to the other diagonal components. But, when particles convecting past each other have an offset in the z-direction, hydrodynamic rotations occur on other axes. Particles translating in the compressional direction with an offset in the z-direction would rotate along the extensional axis, while similar par-

https://doi.org/10.1017/S0022112099006576 Published online by Cambridge University Press

ticles translating along the extensional axis would rotate along the compressional axis. The surplus of particles in the compressional zone causes more particles to translate in the compressional direction – as noted by the negative sign of the translational D_{xy} in this regime – resulting in preferred rotation along the extensional axis, or a positive hydrodynamic contribution to D^r_{xy}. This is an important observation as it verifies the results for the translational D_{xy} with an argument that does not involve exclusion of the affine motion which is unimportant for rotational motion.

6. Summary and concluding remarks

Results for the long-time self-diffusivity have been presented with and without hydrodynamic interactions. Without hydrodynamic interactions, large systems were used enabling accurate results to be obtained for all values of *Pe*, including verification of the $O(Pe)$ and $O(Pe^{3/2})$ corrections to the equilibrium long-time self-diffusivity predicted by Morris & Brady (1996). Qualitative (and semi-quantitative) agreement with the theoretical work of Brady & Morris (1997) was achieved at high *Pe*, with diffusivities scaling like $\dot{\gamma}a^2$. The ϕ-dependence of the diffusivity was also examined. Equilibrium self-diffusivities are decreasing functions of ϕ and agree with the previous results of Cichocki & Hinsen (1992) and Schaertl & Sillescu (1994). Diffusivities at $Pe = 1000$ were found to be strictly increasing functions of ϕ with relative sizes of the diagonal components consistent with the analogy that diffusion is directly related to the stress in this regime.

Inclusion of hydrodynamic interactions adds a configurational- and concentration-dependent particle mobility. In the presence of hydrodynamic interactions we were able to split the diffusivity into its Brownian and hydrodynamic contributions, giving insight into the mechanisms for diffusion over the full range of *Pe*. Brownian diffusion, dominant at low *Pe*, is a random-walk process that is hindered by the presence of other particles. At high shear rates, the prevalent diffusive mechanism is hydrodynamic in origin consisting of displacements due to interactions between neighbouring particles and is thus enhanced by the presence of other particles. Thus, near equilibrium, the diffusivity, scaled by D_0, is found to be a monotonically decreasing function of ϕ, with lower values than in the Brownian Dynamics system. At high *Pe*, each diagonal component of the diffusivity, scaled by $\dot{\gamma}a^2$, grows with ϕ up to a point and then appears to reach a plateau near $\phi \approx 0.50$. It is unclear how this property will behave at higher volume fractions. We were limited to $\phi < 0.50$ due to system size restraints imposed by the computationally intensive Stokesian Dynamics algorithm. Note that the size limitations may affect the values of the diffusivities due to issues associated with fitting the proper microstructure in the small periodic cell even if a very large number of independent runs reduces the statistical noise to near zero.

For the *Pe*-dependence in the Stokesian Dynamic system, very good data were obtained at high shear rates, but we were unable to obtain a good measure of the first correction of the self-diffusivity from equilibrium due to shear. The diffusivity is enhanced by the flow at low *Pe* mainly due to an increase in Brownian diffusion. The hydrodynamic contribution clearly vanishes like Pe^2 at low *Pe* in contrast to the predicted $Pe^{3/2}$ scaling; as was mentioned earlier, the system sizes are too small to fit the $aPe^{-1/2}$ outer length scale necessary to achieve the $Pe^{3/2}$ diffusivity into the simulation cell.

Rotational self-diffusivities are also reported in this work, showing similar behaviour to the translational self-diffusivities. The zz-component is much larger than the other two components as rotation along the z-axis represents rotation in the plane of shear.

https://doi.org/10.1017/S0022112099006576 Published online by Cambridge University Press

Another notable exception is an initial decrease in the rotational diffusivity from its equilibrium value at low shear rates before its linear growth at high shear rates due to hydrodynamic interactions. Unlike the translational diffusivity, the Brownian rotational diffusivity is never enhanced by the flow, being a decreasing function of Pe for all Pe.

This work presents the first known results for colloidal suspensions on the xy-component to the long-time self-diffusion tensor. Two underlying factors dictate the behaviour of this component. First, in shear flow there is a build-up of particles in the compressional zone relative to the extensional zone. Second, as discussed before, Brownian diffusion is hindered by the presence of other particles whereas hydrodynamic diffusion is enhanced. Thus, at low Pe both translation along the compressional axis and rotation around the extensional axis are relatively hindered leading to a positive D_{xy} and a negative D^r_{xy}, respectively. At high Pe, hydrodynamic diffusion takes over but the surplus in the compressional zone remains, thus reversing the signs of both D_{xy} and D^r_{xy}. It would very interesting to see if this off-diagonal diffusivity could be observed in an experiment. Care will be needed to remove the convectively enhanced dispersion which scales as $D_{yy}t^2$ in order to reveal the underlying D_{xy}.

The data for the Brownian Dynamics system are of higher quality and more internally consistent than the Stokesian Dynamics system particularly at high volume fractions and low shear rates. The main reason for this is the size limitations put on the Stokesian Dynamics system due to the high computational cost of this algorithm. In the future, as hardware computational speed increases and Stokesian Dynamics algorithms are improved, it would be interesting to apply the method used to this work to study larger systems at high ϕ and/or low Pe in the presence of hydrodynamic interactions to clarify some issues raised here.

This work was supported in part by grant CTS-9420415 from the National Science Foundation and grant NAG8-1237 from NASA.

REFERENCES

Ball, R. C. & Melrose, J. R. 1995 Lubrication breakdown in hydrodynamic simulations of concentrated colloids. *Adv. Colloid Interface Sci.* **59**, 19.

Barrall, G. A., Schmidt-Rohr, K., Lee, Y. K., Landfester, K., Zimmerman, H., Chingas, G. C. & Pines, A. 1996 Rotational diffusion measurements of suspended colloidal particles using two-dimensional exchange nuclear magnetic resonance. *J. Chem. Phys.* **104**, 509.

Batchelor, G. K. 1977 The effect of Brownian motion on the bulk stress in a suspension of spherical particles. *J. Fluid Mech.* **83**, 97.

Bossis, G. & Brady, J. F. 1984 Dynamic simulation of sheared suspensions. I. General method. *J. Chem. Phys.* **80**, 5141.

Bossis, G. & Brady, J. F. 1987 Self-diffusion of Brownian particles in concentrated suspensions under shear. *J. Chem. Phys.* **87**, 5437.

Bossis, G. & Brady, J. F. 1989 The rheology of Brownian suspensions. *J. Chem. Phys.* **91**, 1866.

Brady, J. F. 1994 The long-time self-diffusivity in concentrated colloidal dispersions. *J. Fluid Mech.* **272**, 109.

Brady, J. F. & Bossis, G. 1988 Stokesian dynamics. *Ann. Rev. Fluid Mech.* **20**, 111.

Brady, J. F. & Morris, J. F. 1997 Microstructure of strongly sheared suspensions and its impact on rheology and diffusion. *J. Fluid Mech.* **348**, 103.

Breedveld, V., Ende, D van den, Tripathi, A. & Acrivos, A. 1998 The measurement of the shear-induced particle and fluid tracer-diffusivities in concentrated suspensions by a novel method. *J. Fluid Mech.* **375**, 297.

https://doi.org/10.1017/S0022112099006576 Published online by Cambridge University Press

Cichocki, B. & Hinsen, K. 1992 Dynamic computer simulation of concentrated hard sphere suspensions. *Physica* A **187**, 145.

Cunha, F. R. da & Hinch, E. J. 1996 Shear-induced dispersion in a dilute suspension of rough spheres. *J. Fluid Mech.* **309**, 211.

Degiorgio, V., Piazza, R. & Jones, R. B. 1995 Rotational diffusion in concentrated colloidal dispersions of hard spheres. *Phys. Rev.* E **52**, 2707.

Dratler, D. I. & Schowalter, W. R. 1996 Dynamic simulation of suspensions of non-Brownian hard spheres. *J. Fluid Mech.* **325**, 53.

Dratler, D. I., Schowalter, W. R. & Hoffman, R. L. 1997 Dynamic simulation of shear thickening in concentrated colloidal suspensions. *J. Fluid Mech.* **353**, 1.

Eckstein, E. C., Bailey, D. G. & Shapiro, A. H. 1977 Self-diffusion of particles in shear flow of a suspension. *J. Fluid Mech.* **79**, 191.

Elrick, D. E. 1962 Source functions for diffusion in uniform shear flow. *Austral. J. Phys.* **15**, 283.

Ermak, D. L. & McCammon, J. A. 1978 Brownian dynamics with hydrodynamic interactions. *J. Chem. Phys.* **69**, 1352.

Foss, D. R. 1999 The rheological behavior of colloidal dispersions: the effects of hydrodynamic interactions. PhD thesis, California Institute of Technology.

Foss, D. R. & Brady J. F. 1999 Brownian Dynamics simulation of hard-sphere colloidal dispersions. *J. Rheol.* (to be submitted).

Heyes, D. M. & Melrose, J. R. 1993 Brownian dynamics simulations of model hard-sphere suspensions. *J. Non-Newtonian Fluid Mech.* **46**, 1.

Jones, R. B. 1989 Rotational diffusion of a tracer colloidal particle. II. Long time orientational correlations. *Physica* A **157**, 752.

Kanetakis, J. & Sillescu, H. 1996 Simultaneous measurement of rotational and translational diffusion by forced Rayleigh scattering. Colloid spheres in suspension. *Chem. Phys. Lett.* **252**, 127.

Kanetakis, J., Tölle, A. & Sillescu, H. 1997 Rotational diffusion of colloid spheres in concentrated suspensions studied by deuteron NMR. *Phys. Rev.* E **55**, 3006.

Leal, L. G. 1973 On the effective conductivity of a dilute suspension of spherical drops in the limit of low particle Péclet number. *Chem. Engng Commun.* **1**, 21.

Leighton, D. T. & Acrivos, A. 1987 Measurement of shear-induced self-diffusion in concentrated suspensions of spheres. *J. Fluid Mech.* **177**, 109.

Melrose, J. R. & Ball, R. C. 1995 The pathological behaviour of sheared hard-spheres with hydrodynamic interactions. *Europhys. Lett.* **32**, 535.

Morris, J. F. & Brady, J. F. 1996 Self-diffusion in sheared suspensions. *J. Fluid Mech.* **312**, 223.

Phan, S. E. & Leighton, D. T. 1993 Measurement of the shear-induced tracer diffusivity in concentrated suspensions. *J. Fluid Mech.*, submitted.

Phillips, R. J., Brady, J. F. & Bossis, G. 1988 Hydrodynamic transport properties of hard-sphere dispersions. I. Suspensions of freely mobile particles. *Phys. Fluids* **31**, 3462.

Rastogi, S. R. 1995 Nonequilibrium Brownian dynamics of colloidal suspensions. PhD thesis, University of Delaware.

Sami, S. 1996 Stokesian dynamics simulations of Brownian suspensions in extensional flow. MS thesis, California Institute of Technology.

Schaertl, W. & Sillescu H. 1994 Brownian dynamics simulations of colloidal hard spheres. Effects of sample dimensionality on self-diffusion. *J. Statist. Phys.* **74**, 687.

Wang, Y., Mauri, R. & Acrivos, A. 1996 Transverse shear-induced diffusion of spheres in a dilute suspension. *J. Fluid Mech.* **327**, 255.

Yurkovetsky, Y. 1998 I. Statistical mechanics of bubbly liquids. II. Behavior of sheared suspensions of non-Brownian particles. PhD thesis, California Institute of Technology.

https://doi.org/10.1017/S0022112099006576 Published online by Cambridge University Press